SANDIA REPORT

SAND2013-9915
Unlimited Release
Printed November 2013

Performance Limits for Maritime Inverse Synthetic Aperture Radar (ISAR)

Armin W. Doerry

Prepared by
Sandia National Laboratories
Albuquerque, New Mexico 87185 and Livermore, California 94550

Sandia National Laboratories is a multi-program laboratory managed and operated by Sandia Corporation, a wholly owned subsidiary of Lockheed Martin Corporation, for the U.S. Department of Energy's National Nuclear Security Administration under contract DE-AC04-94AL85000.

Sandia National Laboratories

Issued by Sandia National Laboratories, operated for the United States Department of Energy by Sandia Corporation.

Available to DOE and DOE contractors from

U.S. Department of Energy
Office of Scientific and Technical Information
P.O. Box 62
Oak Ridge, TN 37831

Telephone: (865) 576-8401
Facsimile: (865) 576-5728
E-Mail: reports@adonis.osti.gov
Online ordering: http://www.osti.gov/bridge

Available to the public from

U.S. Department of Commerce
National Technical Information Service
5285 Port Royal Rd.
Springfield, VA 22161

Telephone: (800) 553-6847
Facsimile: (703) 605-6900
E-Mail: orders@ntis.fedworld.gov
Online order: http://www.ntis.gov/help/ordermethods.asp?loc=7-4-0#online

SAND2013-9915
Unlimited Release
Printed November 2013

Performance Limits for Maritime Inverse Synthetic Aperture Radar (ISAR)

Armin W. Doerry
ISR Mission Engineering
Sandia National Laboratories
P.O. Box 5800
Albuquerque, NM 87185-0519

Abstract

The performance of an Inverse Synthetic Aperture Radar (ISAR) system depends on a variety of factors, many which are interdependent in some manner. In this report we specifically examine ISAR as applied to maritime targets (e.g. ships). It is often difficult to 'get your arms around' the problem of ascertaining achievable performance limits, and yet those limits exist and are dictated by physics. This report identifies and explores those limits, and how they depend on hardware system parameters and environmental conditions. Ultimately, this leads to a characterization of parameters that offer optimum performance for the overall ISAR system.

While the information herein is not new to the literature, its collection into a single report hopes to offer some value in reducing the 'seek time'.

Acknowledgements

This report was funded by General Atomics Aeronautical Systems, Inc. (ASI) Reconnaissance Systems Group (RSG).

Sandia National Laboratories is a multi-program laboratory managed and operated by Sandia Corporation, a wholly owned subsidiary of Lockheed Martin Corporation, for the U.S. Department of Energy's National Nuclear Security Administration under contract DE-AC04-94AL85000.

Contents

Foreword

This report details the results of an academic study. It does not presently exemplify any modes, methodologies, or techniques employed by any operational system known to the author.

Classification

The specific mathematics and algorithms presented herein do not bear any release restrictions or distribution limitations.

This distribution limitations of this report are in accordance with the classification guidance detailed in the memorandum “Classification Guidance Recommendations for Sandia Radar Testbed Research and Development”, DRAFT memorandum from Brett Remund (Deputy Director, RF Remote Sensing Systems, Electronic Systems Center) to Randy Bell (US Department of Energy, NA-22), February 23, 2004. Sandia has adopted this guidance where otherwise none has been given.

This report formalizes preexisting informal notes and other documentation on the subject matter herein.

1 Introduction

Inverse Synthetic Aperture Radar (ISAR) is a radar imaging mode that seeks to employ relatively fine range resolution and Doppler processing to discern target features not otherwise resolvable. In particular, ISAR assumes that the target exhibits angular motion generally independent of, and typically unknown to, the radar. This differentiates it from Synthetic Aperture Radar (SAR) that assumes a static target scene.

ISAR systems have been used to image ships, land vehicles, planes, satellites, asteroids, moons, and planets – basically anything that even appears to move with respect to the radar. In this report we confine our interest to maritime target vessels, i.e. ships, etc.

ISAR performance is dependent on a multitude of parameters, many of which are interrelated in non-linear fashions. Seemingly simple questions such as "What range can we operate at?", "What resolution can we get?", "How fast can we fly?", and "What frequency should we operate at?", are often (and rightly so) hesitantly answered with a slew of qualifiers (ifs, buts, givens, etc.).

These invariably result in performance studies that trade various parameters against each other. Nevertheless, general trends can be observed, and general statements can be made. Furthermore, performance bounds can be generated to offer first order estimates on the achievability of various performance goals. This report attempts to do just this, especially for maritime targets (e.g. ships, etc.).

The ultimate aim of an ISAR system for this report is to image a maritime target vessel, focusing it in spite of unknown target vessel motion as well as possibly known radar motion. A principal radar metric to achieve a useable ISAR image is the Signal-to-Noise (energy) Ratio (SNR) in the ISAR image.

The published literature includes many works on ISAR, but most are detailing image formation algorithms and the like. Very little has been found that speaks to system design issues surrounding the attainment of the raw data that is to be processed into an image. Achieving adequate quality in the raw data is precisely the topic of this report.

Earlier reports performed a similar analysis for SAR performance,[1] and for Ground Moving Target Indicator (GMTI) radar performance.[2] Much of the analysis in this report builds on this earlier work. We will refer to these earlier reports several times hereafter.

“One finds limits by pushing them.”
-- Herbert Simon

2 The Radar Equation

We address here the SNR in the ISAR Range-Doppler (RD) map, or image. A brief recap on the development of this equation is as follows.

For a single pulse, the Received (RX) power at the antenna port is related to the Transmitted (TX) power by

$$P_r = P_t G_A \left(\frac{1}{4\pi R^2} \right) \sigma \left(\frac{1}{4\pi R^2} \right) A_e \left(\frac{1}{L_{radar} L_{atmos}} \right) = \frac{P_t G_A A_e \sigma}{(4\pi)^2 R^4 L_{radar} L_{atmos}}, \tag{1}$$

where

P_r = received signal power (W),
P_t = transmitter signal power (W),
G_A = transmitter antenna gain factor,
A_e = receiver antenna effective area (m^2),
σ = target Radar Cross Section (m^2),
R = range vector from target to antenna (m),
L_{atmos} = atmospheric loss factor due to the propagating wave,
L_{radar} = microwave transmission loss factor due to miscellaneous sources. (2)

The effective noise power that the signal must compete with at the antenna is given approximately by

$$N_r = kTF_N B_N, \tag{3}$$

where

N_r = received noise power (W),
k = Boltzmann's constant = 1.38 x 10-23 J/K,
T = nominal scene noise temperature ≈ 290 K,
F_N = system noise factor for the receiver, and
B_N = noise bandwidth at the antenna port. (4)

Consequently, the Signal-to-Noise (power) ratio at the RX antenna port is effectively

$$SNR_{antenna} = \frac{P_r}{N_r} = \frac{P_t G_A A_e \sigma}{(4\pi)^2 R^4 L_{radar} L_{atmos} (kTF_N) B_N}. \tag{5}$$

A finite data collection time limits the total energy collected, and signal processing in the radar increases the SNR in an ISAR image by two major gain factors. The first is due to pulse compression, and the second is due to coherently combining echoes from multiple pulses, that is, pulse integration. This results in

$$SNR_{image} = SNR_{antenna} G_r G_a = \frac{P_t G_A A_e \sigma \, G_r G_a}{(4\pi)^2 R^4 L_{radar} L_{atmos} (kTF_N) B_N}, \tag{6}$$

where

G_r = SNR gain due to range processing (pulse compression),
G_a = SNR gain due to azimuth processing (coherent pulse integration). (7)

The product $G_r G_a$ comprises the signal processing gain.

This relationship is called “The Radar Equation”.

At this point we examine the image SNR terms and factors individually to relate them to physical ISAR system parameters and performance criteria.

Figure 1. Artist’s concept of General Atomics Sea Avenger UAS. (Courtesy of General Atomics Aeronautical Systems, Inc. All Rights Reserved.)

2.1 Antenna

This report will consider only the monostatic case, where the same antenna is used for TX and RX operation. Consequently, we relate

$$G_A = \frac{4\pi A_e}{\lambda^2}, \tag{8}$$

where λ is the nominal wavelength of the radar. Furthermore, the effective area is related to the actual aperture area by

$$A_e = \eta_{ap} A_A, \tag{9}$$

where

η_{ap} = the aperture efficiency of the antenna, and

A_A = the physical area of the antenna aperture. (10)

Typically, a radar design must live with a finite volume allocated to the antenna structure, so that the achievable antenna physical aperture area is limited. The aperture efficiency takes into account a number of individual efficiency factors, including the radiation efficiency of the antenna, the aperture illumination efficiency of say a feedhorn to a reflector assembly, spillover losses of a feedhorn to a finite reflector area, etc. A typical number for aperture efficiency might be $\eta_{ap} \approx 0.5$.

Putting these into the radar equation yields the expression

$$SNR_{image} = \frac{P_t \left(\eta_{ap}^2 A_A^2\right) \sigma G_r G_a}{(4\pi) R^4 \lambda^2 L_{radar} L_{atmos} (kTF_N) B_N}. \tag{11}$$

2.2 Processing Gains

A detailed discussion of processing gain is given in Appendix A of Reference 1.

The range processing gain is due to noise bandwidth reduction during the course of pulse compression. It is straightforward to show that

$$G_r = \frac{T_{eff} B_N}{L_r}, \tag{12}$$

where

T_{eff} = the effective pulse width of the radar, and

L_r = reduction in SNR gain due to non-ideal range filtering. (13)

Sidelobe reduction in ISAR images is somewhat more important than for SAR. This is because maritime vessels, being man-made objects, often manifest as large collections of specular scatterers with individual scattering centers exhibiting any of a wide range of RCS values. As a result, we are often trying to observe individual pixels in the presence of sidelobes from other bright scatterers. Consequently, in the absence of more refined information, we might typically expect sidelobe filtering with characteristics that include a loss $L_r \approx a_{wr} \approx 1.5$ or so, where a_{wr} is the range impulse response broadening factor due to data weighting or windowing.

The effective pulse width differs from the actual TX pulse width in that the effective pulse width is equal to that portion of the real pulse that makes it into the data set. For digital matched-filter processing they are the same, but for stretch-processing the effective pulse width is typically slightly less than the real transmitted pulse width, but still pretty close. Since maritime ISAR often desires relatively fine resolution, we anticipate that stretch-processing is a viable mode of operation. Furthermore, since maritime ISAR is generally interested in limiting its scene to the immediate neighborhood of the maritime target, we anticipate that pulses will be relatively long, which minimizes the difference between transmitted pulse width and effective pulse width. For the remainder of this report we will optimally presume that the transmitted pulse width is equal to the effective pulse width.

The azimuth processing gain is due to the coherent integration of multiple pulses, otherwise known as Doppler processing. Of course, the total number of pulses that can be collected depends on the radar Pulse Repetition Frequency (PRF) and the Coherent Processing Interval (CPI). Putting all this together yields

$$G_a = \frac{N}{L_a} = \frac{f_p T_{CPI}}{L_a}, \tag{14}$$

where

N = the total number of pulses integrated,
f_p = radar PRF (Hz),
T_{CPI} = Coherent Processing Interval (CPI) time, and
L_a = reduction in SNR gain due to non-ideal Doppler filtering. (15)

Note that for the same reasons as with range processing, in the absence of more refined information, typically $L_a \approx a_{wa} \approx 1.5$ or so, where a_{wa} is the Doppler impulse response broadening factor due to data weighting or windowing.

Putting these into the radar equation yields

$$SNR_{image} = \frac{P_t T_{eff} f_p T_{CPI} \left(\eta_{ap}^2 A_A^2\right) \sigma}{(4\pi) R^4 \lambda^2 (kTF_N) L_{radar} L_{atmos} L_r L_a}. \quad (16)$$

Maritime Vessel Dynamics

In addition, Doppler resolution is inversely proportional to T_{CPI}, although it also depends on the non-ideal azimuth filtering to control sidelobes. There is a tacit presumption in this equation that the target itself remains coherent over the desired T_{CPI}.

Typical ISAR processing furthermore normally assumes that a target's scatterers exhibit linear range changes during the CPI. An analysis of typical ship motion shows for a typical ship that is pitching and rolling, it is therefore difficult to justify a CPI length longer than 2 to 3 seconds.[3,4]

While we can accurately resolve Doppler, unlike SAR, Doppler does not necessarily correspond to an azimuth position. It may not even correspond to an azimuth direction. This is because the target vessel exhibits its own motion that is unknown to the radar. This contributes to the "blobology" nature of typical ISAR images.

The impact of ship motion on PRF selection is discussed later in this report.

2.3 The Transmitter

The transmitter is generally specified to first order by 3 main criteria:

1) The frequency range of operation,

2) The peak power output (averaged during the pulse on-time), and

3) The maximum duty factor allowed.

We identify the duty factor as

$$d = T_{eff}\, f_p = \frac{P_{avg}}{P_t}, \tag{17}$$

where P_{avg} is the average power transmitted during the CPI collection period. Consequently, we identify

$$P_t T_{eff}\, f_p = P_t d = P_{avg}. \tag{18}$$

Transmitter power capabilities and bandwidths are very dependent on transmitter technology. In general, for tube-type power amplifiers, higher power generally implies lesser capable bandwidth, and hence lesser range resolution. The signal bandwidth required for a particular range resolution for a single pulse is given by

$$B_T = \frac{a_{wr} c}{2\rho_r}, \tag{19}$$

where

ρ_r = slant-range resolution required,
a_{wr} = range impulse response broadening factor,
c = velocity of propagation. (20)

There is no typical duty factor that characterizes all, or even most, power amplifiers. Duty factors may range from on the order of 1% to 100% across the variety of power amplifiers available. Typically, a maximum duty factor needed by a pulse-Doppler radar is less than 50%, and usually less than about 35% or so. Consequently, a reasonable duty

factor limit of 35% might be imposed on power amplifiers that could otherwise be capable of more. [1]

In practice, the duty factor limit for a particular power amplifier may not always be achieved due to timing constraints for the geometry within which the radar is operating, but we can often get pretty close.

We take this opportunity to also note that wavelength is related to frequency as

$$\lambda = \frac{c}{f}, \tag{21}$$

where f is the radar nominal frequency.

A discussion of representative power amplifier tube capabilities can be found in Reference 1.

In any case, we now refine the radar equation to be

$$SNR_{image} = \frac{P_{avg} T_{CPI} \left(\eta_{ap}^2 A_A^2\right) f^2 \sigma}{(4\pi) c^2 R^4 (kTF_N) L_{radar} L_{atmos} L_r L_a}, \tag{22}$$

noting that the average power is based on the power amplifier's duty factor limit. For wideband radar systems this might be limited to perhaps 35%, but can often be far less.

[1] We are omitting discussion of FMCW radars beyond noting that their duty factor is typically 100%, with *effective* duty factor sometimes somewhat less. This does come at a price of reduced antenna aperture size limits, owing to separate transmit and receive apertures required to maintain isolation, a fact often ignored by FMCW proponents.

2.4 The Target Radar Cross Section (RCS)

The RCS of a target denotes its ability to reflect energy back to the radar.

A maritime ISAR target is a fairly complex target, exhibiting fairly complex radar scattering characteristics. However we may state some inescapable truths.

- Maritime vessels tend to be constructed of metal, with many facets, corners and edges, albeit on a scale comparable with the radar resolution. Consequently, they embody numerous specular scattering centers, as opposed to being characterized with distributed reflectivity like a vegetation field.

- We desire to operate with range and Doppler resolution that is much finer than the dimensions of the typical maritime target vessel itself. That is, we wish to resolve multiple, in fact many, scattering centers on the target vessel. Their relative position will help define the vessel's shape and large-scale features.

- We desire to not only resolve the specular scattering centers, but clearly discern them from surrounding clutter and noise.

These observations conspire to suggest that we treat the radar equation analysis as desiring some minimum SNR for some minimum scattering center RCS. The question then becomes "What should the minimum RCS be for an adequate amount of SNR?"

We may refine this question into an equivalent question "What RCS should yield an SNR of 0 dB?" That is, what should be the equivalent RCS of the average noise level? This is very much the same as for specifying GMTI noise-equivalent RCS.

We note that for specular (non-distributed) targets, a variety of frequency dependencies exists, and are characterized in the following table.

Table 1. RCS frequency dependence.

target characteristic	examples	frequency dependence
2 radii of curvature	spheroids	None
1 radius of curvature	cylinders, top hats	f
0 radii of curvature	flat plates, dihedrals, trihedrals	f^2

Distributed targets tend to exhibit a frequency dependence approximately proportional to frequency f.

To meaningfully compare a radar's performance at other frequencies for the same target, the target's frequency dependency must be accounted for. We do this by equating

$$\sigma = \sigma_{ref} \left(\frac{f}{f_{ref}} \right)^n , \tag{23}$$

where

n = some power, not necessarily an integer. (24)

The implication is that for many scattering centers, any one scattering center might often be dimmer at lower frequencies, and brighter at higher frequencies. While these behaviors apply to these simple targets, we need to remember that complicated targets may have considerably more complicated frequency dependence.

We might expect that a maritime vessel is comprised of all kinds of scattering centers with a wide variety of curvature characteristics. In the absence of further information, we might just simply assume a representative linear relationship ($n = 1$).

Nevertheless, folding the RCS dependencies into the radar equation, and rearranging a bit, yields

$$SNR_{image} = \frac{P_{avg} T_{CPI} \left(\eta_{ap}^2 A_A^2 \right) \sigma_{ref} \left(\frac{f}{f_{ref}} \right)^n f^2}{(4\pi) c^2 R^4 (kTF_N) L_{radar} L_{atmos} L_r L_a} . \tag{25}$$

Maritime Vessel RCS Distributions

The question we really need to answer is "What should be the RCS equivalent of the average noise level, so that the target vessel's collection of scattering centers exhibit sufficient SNR that we might draw useful intelligence about the 'shape' and other features of the target vessel?"

Ample literature exists that describes the RCS of maritime vessels as a single reflecting entity, that is, the RCS of the entire ship as might be useful for Maritime Wide Area Search (MWAS) modes. However, for our ISAR images, we need to resolve many individual scattering centers distributed over the entire vessel. Furthermore, we need a large number of these scattering centers to be 'visible' in the ISAR image, that is, with adequate SNR so that they can be in fact detected and identified as scattering centers. We expect most of these individual scattering centers to exhibit a local RCS that is substantially less than their combined 'whole ship' RCS. We in fact desire to know the RCS statistics of a typical vessel's scattering centers. This will aid us in setting a threshold for RCS that we want to be visible with adequate SNR.

RCS characteristics for complex targets are ascertained typically in one of the following three ways.

1. Direct measurements of real target vessels. This would most likely be from actual flight test data.

2. Measurements of scaled models of target vessels. This is often from ISAR turn-table measurements.

3. Computer simulation using computer models. Electromagnetic modeling and simulation tools such as Xpatch are often used for this. The various tools available offer varying degrees of fidelity (also requiring varying degrees of computational horsepower).

With any luck, someone else would have already done one or more of these for us, and dutifully reported it in the accessible literature. An examination of the published literature, however, has not yielded suitable data at this time. In spite of the need, a comprehensive study to yield high-confidence statistical data is beyond the scope of this report. Consequently, we resort to anecdotal and heuristic data.

Furthermore, we will answer a slightly different question, namely "How high can be the average noise level, so that we can still render a reasonably good 'image' of a representative target vessel?"

For Ku-band, the anecdotal answer seems to be an average noise level in the neighborhood of 0 dBsm will still allow reasonably useful renderings of large ships; those with RCS of perhaps +40 dBsm or more. We refer the reader to Appendix A for a justification for this.

For smaller vessels, anecdotal evidence suggests that a noise level perhaps 40 dB below the peak RCS of the vessel will allow adequate SNR for a sufficient number of vessel features to allow useable rendering. This allows for at least a 10 dB SNR for all features within 30 dB of the peak RCS value.

RCS Calibration

We briefly comment here that maritime vessel classification, and perhaps even identification, may depend on the expected RCS of a target of interest, or its features. Consequently, an accurate RCS measure facilitates proper target characterization for these ends.

An accurate RCS measure requires a complete understanding of the gains and losses in an ISAR system, and adequate compensation of them. An ISAR system therefore should be radiometrically calibrated.

2.5 Radar Geometry

Typically, the radar is specified to operate at a particular height, and directed to image a vessel at some specified geographical location, with some corresponding range from the radar. The height and range are the necessary geometric entities to calculate SNR in the ISAR image.

The range is overtly represented in the radar equation.

Both range and radar altitude are also present, albeit somewhat hidden, in the atmospheric loss parameter. This will be discussed in a later section.

We do note that particularly at long ranges atmospheric refractive effects will cause a noticeable difference between geometric range and 'electrical' range, that is, the range calculated from an echo time delay.[5] We opine, however, that the size of the target vessel, combined with the uncertainty of its motion, will conspire to render the significance of the range error to essentially inconsequential. That is, we probably don't need to worry about it.

Figure 2. The guided-missile destroyer USS Milius (DDG 69) on a routine deployment in the Arabian Gulf, 18 March 2012. (U.S. Navy photo by Ens. Robert Kelly)

2.6 SNR Losses and Noise Factor

The radar equation as presented notes several broad categories of SNR losses.

2.6.1 Signal Processing Losses

Signal processing losses include the SNR loss (relative to ideal processing gains) due to employing a window taper function for sidelobe control. Recall that the window bandwidth (including its noise bandwidth) is increased somewhat. If window functions are incorporated in both dimensions (range and Doppler processing), then we incur a SNR loss typically slightly larger than the impulse response broadening factor, perhaps on the order of 1.5 dB for each dimension.

In particular, the range processing SNR loss due to using a window function can be mitigated by using a waveform with an autocorrelation function that already exhibits the desired sidelobe characteristics. One such class of waveforms are the Non-Linear FM (NLFM) waveforms.[6,7] Similar performance can be had by manipulating statistics of random-phase radar waveforms.[8,9] This would save the typical 1.5 dB that is otherwise lost.

For specular target features we might also incorporate an additional 'straddling' loss due to a target not being centered in a resolution cell. This depends on the relationship of pixel spacing to resolution, also known as the oversampling factor, but might be as high as 3 dB.

2.6.2 Radar Losses

Radar losses include a variety of losses primarily over the microwave signal path, but doesn't include the atmosphere. Included are a power loss from transmitter power amplifier output to the antenna port, and a two-way loss through the radome. These are generally somewhat frequency dependent, being higher at higher frequencies, but major effort is expended to keep them both as low as is reasonably achievable. In the absence of more refined information, typical numbers might be 0.5 dB to 2 dB from TX amplifier to the antenna port, and perhaps an additional 0.5 dB to 1.5 dB two-way through the radome.

2.6.3 System Noise Factor

When the system noise factor is expressed in dB, it is often referred to as the system noise figure.

The system noise figure includes primarily the noise figure of the front-end Low-Noise Amplifier (LNA) and the losses between the antenna and the LNA. These both are a function of a variety of factors, including the length and nature of cables required, LNA protection and isolation requirements, and of course frequency. Frequency dependence is generally such that higher frequencies will result in higher system noise figures. For

example, typical system noise figures for sub-kilowatt radar systems are 3.0 dB to 3.5 dB at X-band, 3.5 dB to 4.5 dB at Ku-band, and perhaps 6 dB at Ka-band.

2.6.4 Atmospheric Losses

Atmospheric losses depend strongly on frequency, range, and the nature of the atmosphere (particularly the weather conditions) between radar and target. Major atmospheric loss factors are atmospheric density, humidity, cloud water content, and rainfall rate. These conspire to yield a 'loss-rate' often expressed as dB per unit of distance, that is very altitude and frequency dependent. The loss-rate generally increases strongly with frequency, but decreases with radar altitude, owing to the signal path traversing a thinner average atmosphere.

A typical radar specification is to yield adequate performance in an atmosphere that includes weather conditions supporting a 4 mm/Hr rainfall rate on the ground.

We identify the overall total atmospheric loss as

$$L_{atmos} = 10^{\frac{\alpha R}{10}}, \tag{26}$$

where α = the two-way atmospheric loss rate in dB per unit distance.

Nominal two-way loss rates from various altitudes for some surface rain rates are listed in the following tables. While numbers listed are to several significant digits, these are based on a model and are quite squishy.[10,11]

Incorporating atmospheric loss-rate overtly into the radar equation, and rearranging a bit, yields

$$SNR_{image} = \frac{P_{avg} T_{CPI} \left(\eta_{ap}^2 A_A^2\right) \sigma_{ref} \left(\frac{f}{f_{ref}}\right)^n f^2}{(4\pi) c^2 (kTF_N)(L_{radar} L_r L_a) R^4 10^{\frac{\alpha R}{10}}}. \tag{27}$$

Implicit in the radar equation is that the atmospheric loss-rate depends on *f* in a decidedly nonlinear manner (and not necessarily even monotonic near specific absorption bands – of note are an H_2O absorption band at about 23 GHz, and an O_2 absorption band at about 60 GHz).

Table 2. Two-way loss rates (dB/km) in 50% RH clear air.

Radar Altitude (kft)	L-band 1.5 GHz	S-band 3.0 GHz	C-band 5.0 GHz	X-band 9.6 GHz	Ku-band 16.7 GHz	Ka-band 35 GHz	W-band 94 GHz
5	0.0119	0.0138	0.0169	0.0235	0.0648	0.1350	0.7101
10	0.0110	0.0126	0.0149	0.0197	0.0498	0.1053	0.5357
15	0.0102	0.0115	0.0133	0.0170	0.0400	0.0857	0.4236
20	0.0095	0.0105	0.0120	0.0149	0.0333	0.0721	0.3476
25	0.0087	0.0096	0.0108	0.0132	0.0282	0.0616	0.2907
30	0.0080	0.0088	0.0099	0.0119	0.0246	0.0541	0.2515
35	0.0074	0.0081	0.0090	0.0108	0.0218	0.0481	0.2214
40	0.0069	0.0075	0.0083	0.0099	0.0196	0.0434	0.1977
45	0.0064	0.0069	0.0076	0.0090	0.0176	0.0392	0.1774
50	0.0059	0.0064	0.0071	0.0083	0.0161	0.0360	0.1617

Table 3. Two-way loss rates (dB/km) in 4 mm/Hr (moderate) rainy weather.

Radar Altitude (kft)	L-band 1.5 GHz	S-band 3.0 GHz	C-band 5.0 GHz	X-band 9.6 GHz	Ku-band 16.7 GHz	Ka-band 35 GHz	W-band 94 GHz
5	0.0135	0.0207	0.0502	0.1315	0.5176	2.1818	8.7812
10	0.0126	0.0193	0.0450	0.1107	0.4062	1.7076	7.7623
15	0.0117	0.0175	0.0391	0.0920	0.3212	1.3311	6.4537
20	0.0106	0.0150	0.0314	0.0714	0.2453	1.0082	4.8836
25	0.0096	0.0132	0.0264	0.0584	0.1979	0.8108	3.9218
30	0.0088	0.0118	0.0228	0.0496	0.1662	0.6788	3.2796
35	0.0081	0.0107	0.0201	0.0431	0.1433	0.5838	2.8178
40	0.0074	0.0098	0.0180	0.0382	0.1259	0.5122	2.4701
45	0.0069	0.0089	0.0163	0.0342	0.1121	0.4558	2.1967
50	0.0064	0.0082	0.0149	0.0310	0.1012	0.4109	1.9793

Table 4. Two-way loss rates (dB/km) in 16 mm/Hr (heavy) rainy weather.

Radar Altitude (kft)	L-band 1.5 GHz	S-band 3.0 GHz	C-band 5.0 GHz	X-band 9.6 GHz	Ku-band 16.7 GHz	Ka-band 35 GHz	W-band 94 GHz
5	0.0166	0.0373	0.1531	0.4910	1.8857	7.3767	23.0221
10	0.0159	0.0347	0.1282	0.3829	1.4091	5.6330	21.0363
15	0.0146	0.0307	0.1060	0.3020	1.0738	4.3037	17.7448
20	0.0128	0.0249	0.0816	0.2289	0.8097	3.2377	13.3520
25	0.0113	0.0211	0.0665	0.1844	0.6459	2.5944	10.6964
30	0.0102	0.0184	0.0563	0.1546	0.5425	2.1651	8.9251
35	0.0093	0.0163	0.0488	0.1331	0.4658	1.8578	7.6569
40	0.0085	0.0147	0.0431	0.1169	0.4081	1.6269	6.7043
45	0.0078	0.0133	0.0386	0.1042	0.3630	1.4467	5.9604
50	0.0073	0.0122	0.0349	0.0940	0.3270	1.3027	5.3667

Figure 3. The amphibious assault ship USS Bataan (LHD 5) returning from pre-deployment training exercise with U.S. Marines to Naval Station Norfolk, 23 May 2013. (U.S. Navy photo by Mass Communication Specialist 1st Class Phil Beaufort)

2.7 Other Useful Expressions and Observations

The radar equation comes in a plethora of versions based on different parameters. We begin with the expression

$$SNR_{image} = \frac{P_{avg} T_{CPI} \left(\eta_{ap}^2 A_A^2\right) \sigma_{ref} \left(\frac{f}{f_{ref}}\right)^n f^2}{(4\pi) c^2 (kTF_N)(L_{radar} L_r L_a) R^4 10^{\frac{\alpha R}{10}}}. \tag{28}$$

Another useful variant expression is

$$SNR_{image} = \left(\frac{P_{avg} G_A^2 \lambda^2 T_{CPI} \sigma_{ref}}{(4\pi)^3 (kTF_N) R^4}\right)\left(\frac{1}{L_{radar} 10^{\frac{\alpha R}{10}}}\right)\left[\frac{1}{L_r L_a}\right]\left[\frac{f}{f_{ref}}\right]^n. \tag{29}$$

Some useful observations include

- PRF can be traded for pulse width to keep P_{avg} constant.
- SNR does not depend on range resolution (for specular reflectors modeled as point targets).
- SNR does depend on Doppler resolution. Finer Doppler resolution requires larger T_{CPI}, which improves SNR.
- There is no SNR overt dependence on grazing angle, although σ_{ref} itself may exhibit some dependence on grazing angle as previously discussed, and atmospheric loss depends on height and range.
- Input Noise bandwidth B_N has no direct effect on ultimate image SNR. Signal bandwidth does not explicitly impact SNR directly, but rather through a looser dependence on perhaps L_r.

2.8 Grouping Parameters due to Geometry, Hardware, and Processing

Influential parameters can be divided into three principal categories, namely

1. Radar operating geometry,
2. Radar hardware limitations, and
3. Radar signal processing.

We now examine the radar equation with respect to these categories. The Radar Equation in the previous development can easily be manipulated to be

$$SNR_{image} = \frac{P_{avg} G_A^2 \lambda^2 T_{CPI} \sigma}{(4\pi)^3 (kTF_N) R^4 L_{radar} L_{atmos} L_r L_a}. \tag{30}$$

Rather than specifying the image SNR with respect to some target scene RCS, the radar equation for ISAR can be written in a manner that assumes that image SNR is unity for some target RCS. Indeed, the achievable 'Noise Equivalent' RCS can be calculated as

$$\sigma_N = \frac{\sigma}{SNR_{image}} = \frac{(4\pi)^3 (kTF_N) R^4 L_{radar} L_{atmos} L_r L_a}{P_{avg} G_A^2 \lambda^2 T_{CPI}}. \tag{31}$$

This is an analogous measure to Noise Equivalent Reflectivity for SAR systems. It recognizes that building a radar to achieve 0 dB SNR for a 0 dBsm RCS target is the same radar to achieve 5 dB SNR for a +5 dBsm RCS, or a 10 dB SNR for a +10 dBsm RCS. Specific thresholds for SNR or RCS depend on processing choices. What is achievable depends on their ratio as allowed by the underlying data. Generally, this 'Noise Equivalent' RCS number is desired to be as low as possible. Range limits of the ISAR will be set based on some threshold for this 'Noise Equivalent' RCS.

To facilitate the subsequent discussion, we may rewrite this equation with parameters grouped as

$$\sigma_N = 64\pi^3 kT \left(\frac{R^4}{T_{CPI}} \right) \left(\frac{F_N L_{radar} L_{atmos}}{P_{avg} G_A^2 \lambda^2} \right) (L_r L_a). \tag{32}$$

The parameters preceding the parentheses are constants that will not be discussed any further.

Radar operating geometry

The first set of parameters $\left(R^4/T_{CPI}\right)$ deal with the radar platform's physical relationship with respect to the target scene. This is about where the radar is and what it is looking at. These parameter are important to the radar designer as it certainly impacts the needed functionality of the hardware design, in particular timing and control, but otherwise is not controllable by the radar hardware designer.

We have included T_{CPI} here because it is often limited by target vessel motion dynamics, which is of course a dynamic geometry thing.

Radar hardware limitations

The second set of parameters $\left(F_N L_{radar} L_{atmos}\right)/\left(P_{avg} G_A^2 \lambda^2\right)$ deal with radar hardware limitations. These need to be selected by a hardware designer based on the limitations of radar geometry and environment, but mindful of the needs of the radar signal processing. The purpose of the hardware is to provide usable data to the signal processor, but otherwise cannot control how the signal processor chooses to specifically process the data into an image.

Radar wavelength λ is a fundamental parameter of the hardware. The antenna gain G_A is normally fixed by its construction. The transmitter is limited by its hardware to some maximum P_{avg}, although it may be specified via a maximum peak transmitter power with some maximum duty factor. The radar duty factor, in turn, is proportional to both radar PRF and pulse width. Some radar geometries may affect allowable duty factors and hence P_{avg}, but achievable P_{avg} under these circumstances is still a radar hardware design limitation. The receiver will also exhibit some noise figure F_N that is a function of its construction.

Hardware system losses are embodied in L_{radar}. The atmospheric propagation loss L_{atmos} is a function of geometry, but is also a function of the radar operating wavelength λ. More commonly, a weather model is specified for the radar that is wavelength independent (e.g. clear air, or must accommodate 4 mm/Hr rain, etc.) When a weather model is specified, in addition to the geometry, then the radar designer does have some control over the specific value for L_{atmos} via selecting the radar wavelength.

Radar signal processing

The third set of parameters $(L_r L_a)$ deal with signal processing issues in the image formation processor. Fundamental limits exist within the data on achievable σ_N. These can, of course, always be made worse with signal processing, but not better than the hardware-limited data can support.

The nature of range sidelobe filtering will coarsen range resolution by the factor a_{wr}, and reduce the range processing gain with respect to ideal matched filtering by a factor L_r. Similarly, the nature of Doppler sidelobe filtering will coarsen azimuth resolution by the factor a_{wa}, and reduce the azimuth processing gain with respect to ideal matched filtering by a factor L_a.

Figure 4. USS Tempest (PC-2) was the second Cyclone-class Patrol (coastal) ship, length 53 m, beam 7.6 m, maximum speed 32 kts. (image courtesy US Navy)

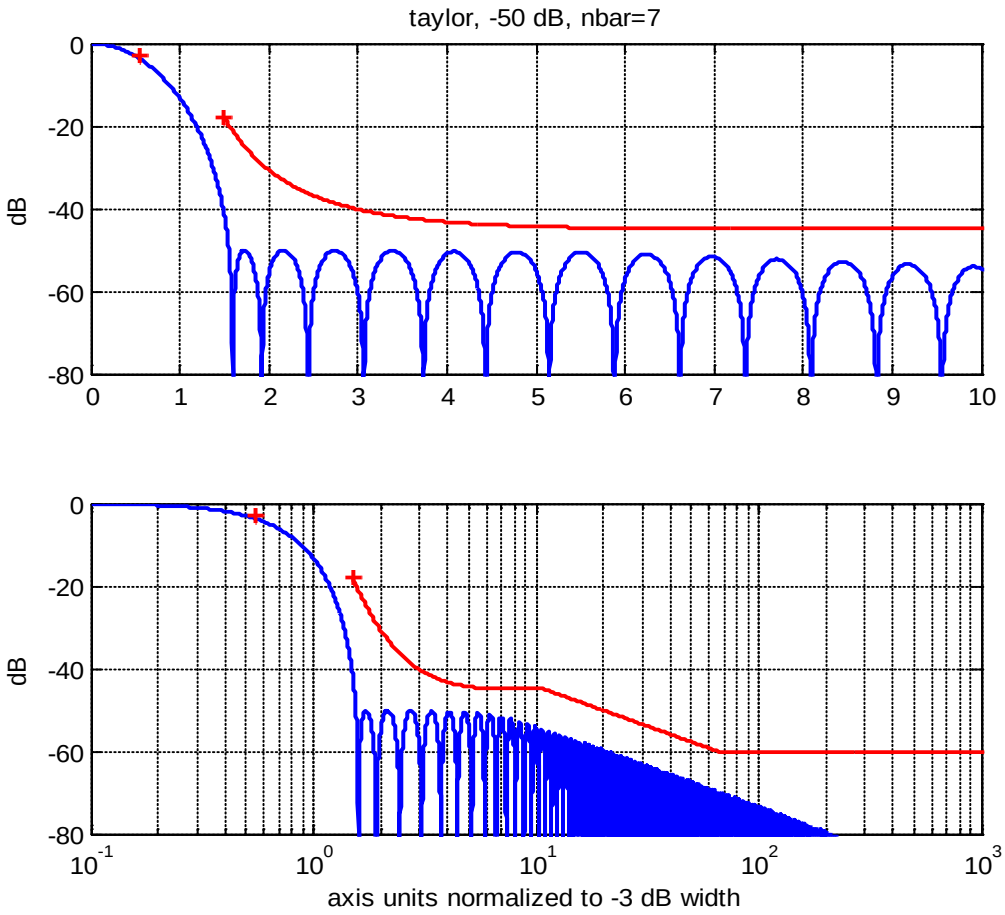

window IPR -3 dB bin bandwidth = 1.3599 (corresponds to sinc width of 0.8845)
window IPR -18 dB rel bandwidth = 2.2755 (normalized to -3 dB width)
window IPR first null = 1.5942 (normalized)
window SNR gain = -1.5421 dB
window PSL = -50.0746 dBc
window ISL = -39.9325 dBc from 1.5942 outward

Figure 5. Example window taper function with metrics.

3 Performance Issues

What follows is a discussion of several issues impacting performance of an ISAR system.

3.1 Optimum Frequency

For this report, the optimum frequency band of operation is that which yields the maximum SNR in the image for the targets of interest.

For constant average transmit power, constant antenna aperture, constant CPI time, constant velocity, and constant system losses, the SNR in the range-Doppler map is proportional to

$$SNR_{image} \propto \frac{f^{(n+2)} 10^{\frac{-\alpha R}{10}}}{R^4}. \tag{33}$$

where atmospheric loss rate α also depends on frequency (generally increasing with frequency as previously discussed). Clearly, for any particular range *R*, some optimum frequency exists to yield a maximum SNR in the image.

Additionally, the optimum frequency will depend somewhat on the RCS characteristic of the target, that is, the frequency dependence *n*. Trihedral features may exhibit an $n = 2$ characteristic, whereas long nearly linear edges would be expected to offer something more like an $n = 1$ characteristic.

Figure 6 through Figure 9 indicate the relative SNR in the ISAR image as a function of slant-range for various frequency bands.

We note that 1 nmi (nautical mile) = 1.852 kilometers, and 1 kft = 304.8 meters. Furthermore, 1 kt = 0.5144 m/s approximately.

In summary, for a constant real antenna aperture size, antenna gain increases with frequency, as does brightness of the target (at least for simple targets). However, as range increases, atmospheric losses increase correspondingly and more so at higher frequencies, eventually overcoming any advantage due to antenna gain and target brightness. Consequently, for any particular atmosphere, radar height and range, there exists an optimum frequency band for ISAR operation. Generally, as range increases and/or weather gets worse, lower frequencies become more attractive. We do note that the target RCS brightness can be a fairly complicated function of frequency, and will depend on the environment within which we wish to detect it, but this is difficult to account for in comparative trade studies, driving us to use simpler models for RCS frequency dependence. Optimal ISAR frequencies for a typical weather specification are illustrated in Figure 10.

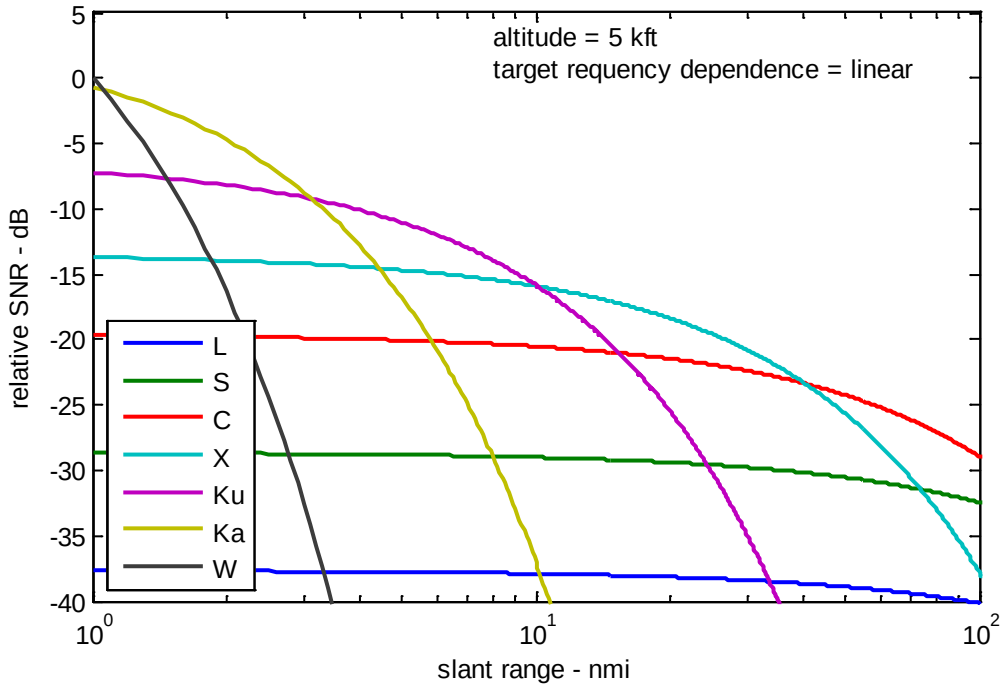

Figure 6. ISAR relative performance of radar bands as a function of range (4 mm/Hr rain, 5 kft altitude, n=1).

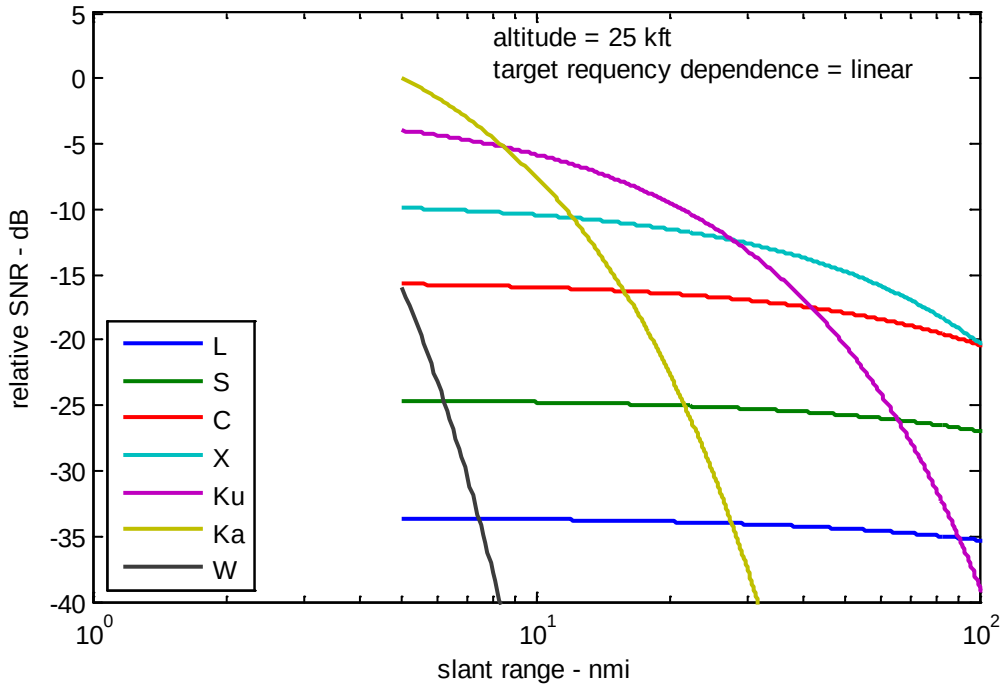

Figure 7. ISAR relative performance of radar bands as a function of range (4 mm/Hr rain, 25 kft altitude, n=1).

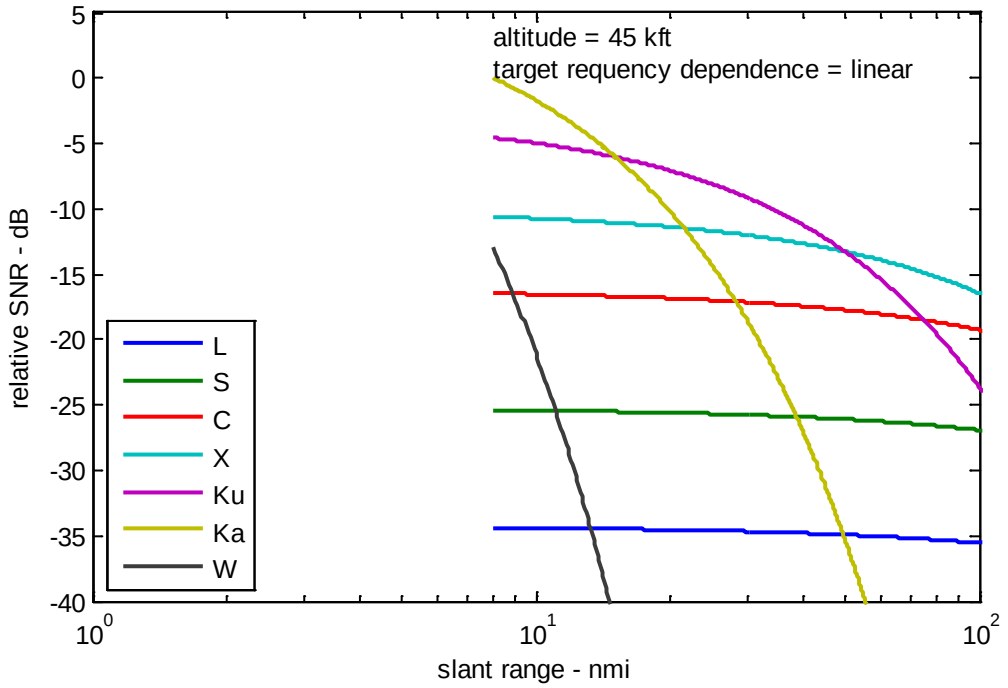

Figure 8. ISAR relative performance of radar bands as a function of range (4 mm/Hr rain, 45 kft altitude, n=1).

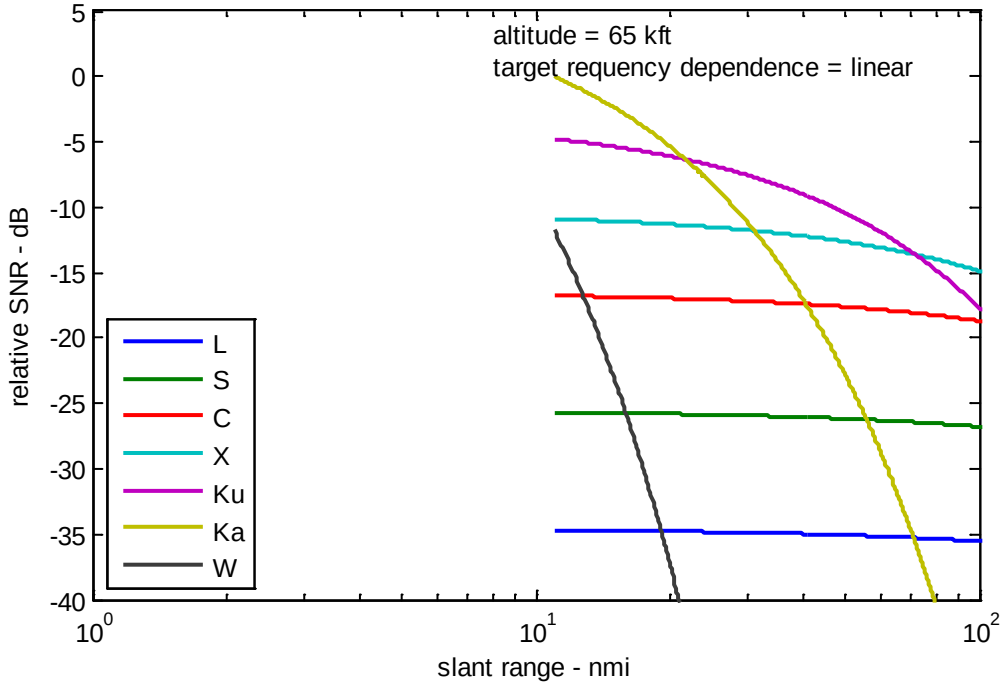

Figure 9. ISAR relative performance of radar bands as a function of range (4 mm/Hr rain, 65 kft altitude, n=1).

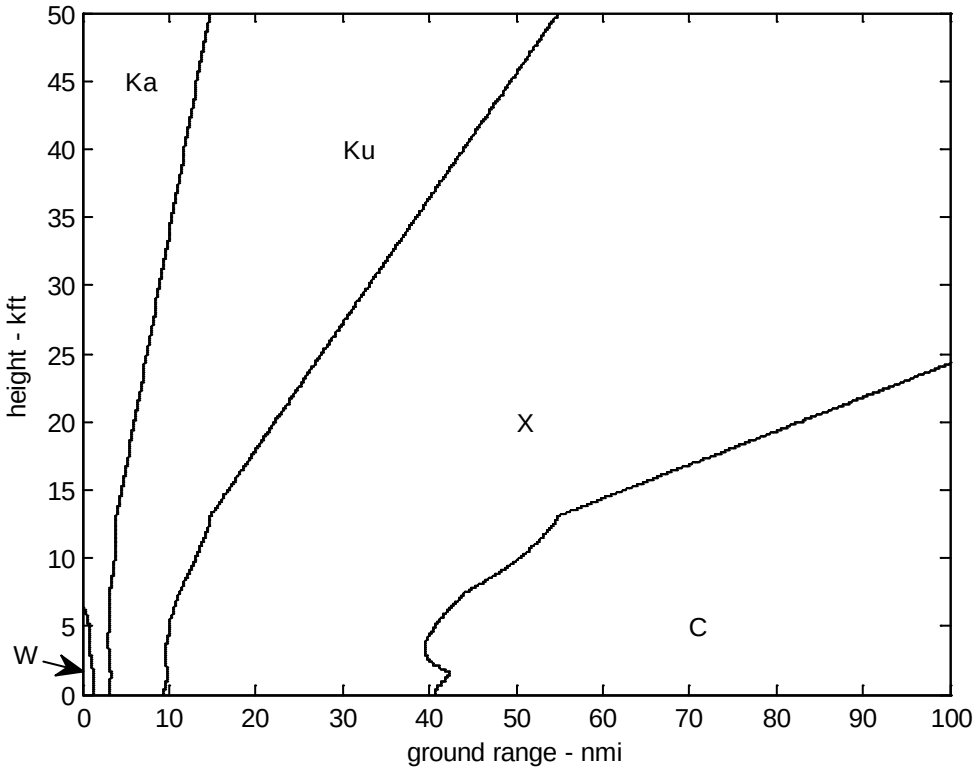

Figure 10. Optimum ISAR radar band as a function of range and altitude (4mm/Hr rain, n=1, constant antenna aperture area).

It should be noted that other reasons (besides optimal SNR) may exist for choosing a particular radar band for operation (e.g. spectral compatibility, pre-existing hardware, hardware availability, ATR template compatibility, program directive, etc.). We also recall that for some targets, a lower frequency may allow a longer target coherence time.

3.2 Radar Pulse Repetition Frequency (PRF)

A target vessel will exhibit both bulk translational motion, and angular motion, as viewed by the radar. The bulk translational motion is of interest for tracking the vessel position and estimating its velocity. However, it is the angular motion that allows us to resolve vessel features, and create the ISAR image. The Doppler due to the bulk translational motion is generally compensated during the ISAR data collection and/or image formation process.

The essence of ISAR is nevertheless that a target vessel will itself exhibit its own motion. In fact, we rely on angular motion of the vessel to generate the Doppler spread of the target, allowing us to resolve vessel features in Doppler.

The principal motions that concern us with respect to discerning maritime target vessel features are roll and pitch. These tend to be modeled as sinusoidal in nature, with periods depending on the dimensions and construction of the ship.

We model the pitch and roll angles as

$$\phi_p = \theta_{p,\max} \sin\left(\frac{2\pi}{T_p} t\right) = \text{instantaneous pitch angle, and}$$

$$\phi_r = \theta_{r,\max} \sin\left(\frac{2\pi}{T_r} t\right) = \text{instantaneous roll angle,} \tag{34}$$

where

$\theta_{r,\max}$ = maximum roll angle,
T_r = roll period,
$\theta_{p,\max}$ = maximum pitch angle, and
T_p = pitch period. (35)

From a distant radar, with generally a low grazing angle perspective, the tallest part of the ship is most likely to exhibit the greatest line-of-sight velocity, and hence Doppler shift in the ISAR image. Accordingly, the respective Doppler shifts with respect to the center of the maritime vessel would be calculated as

$$f_{d,pitch,\max} = \frac{4\pi\, h\theta_{p,\max}}{\lambda T_p} = \text{max observed Doppler due to pitch, and}$$

$$f_{d,roll,\max} = \frac{4\pi\, h\theta_{r,\max}}{\lambda T_r} = \text{max observed Doppler due to roll,} \tag{36}$$

where in this case

h = height of tallest point on the ship. (37)

Over any respective period, the observed Doppler offset will oscillate sinusoidally between positive and negative of these limits.

Although for a typical mono-hull ship, the pitch period is 1/3 to 2/3 that of the roll period, the maximum roll angle is typically several times the maximum pitch angle. These conspire to generally cause the maximum observed Doppler to be due to roll instead of pitch. Of course the actual observed Doppler will be very aspect dependent. But it remains true that Doppler due to roll observed from a worst-case broadside perspective will generally be greater than Doppler due to pitch observed from a worst-case fore/aft perspective.

We examine several examples:

> A typical Navy destroyer might be 150 m long, with a mast height of perhaps 30 m, and exhibit a roll period of 10 sec. In Sea-State 4, this might exhibit a typical roll angle of less than 10 degrees. A Ku-band radar ($\lambda = 0.018$ m) will see a maximum Doppler offset due to roll of 366 Hz.
>
> A typical aircraft carrier might be 300 m long, with a mast height of perhaps 60 m, and exhibit a roll period of 16 sec. In very heavy seas, this might exhibit a roll angle of up to 30 degrees. A Ku-band radar ($\lambda = 0.018$ m) will then see a maximum Doppler offset due to roll of 1371 Hz.

Similar numbers are calculated for large commercial ships, e.g. container ships, tankers, etc.

Since the instantaneous Doppler shift will oscillate between positive and negative maximum values, the Doppler spectrum over time will be twice the maximum Doppler offset. To avoid aliasing, the radar PRF needs to be no less than the Doppler spectrum width.

This suggests that a radar PRF of 1 kHz will suffice much of the time for a Ku-band radar, but for heavy seas needs to be increased to perhaps 2 kHz or more. These limits might be, or may need to be, adjusted for other radar bands.

3.3 Radar Range Resolution

A typical criterion for target classification is on the order of 50 to 100 “pixels on target”.

We shall transmogrify this to the desire for a range resolution of no coarser than 1/50 to 1/100 of the vessel length for the type of vessel we wish to query or image. We do note that even if pixels are not observable over the entire interval of the vessel’s length, that the vessel also has width which affords additional opportunity for observable pixels. Furthermore, we do expect that the vessel’s ISAR image has both range and Doppler non-zero extent.

This suggests the following table.

Table 5. Desired Range Resolution.

Length of target vessel to be imaged (typical classes)	*Maximum (coarsest) desired resolution*
Length > 150+ m (Large freighter, destroyers, aircraft carrier)	3 m
50 m < Length < 150 m (commercial fishing, frigate, Littoral Combat Ships)	1 m
Length < 50 m (commercial fishing, USCG Cutters, coastal patrol craft)	0.3 m

As of this writing, the largest ship ever in service was the super-tanker Mont (originally the Seawise Giant), with an overall length of 458.45 m. Currently the Maersk Triple E class family of large, fuel-efficient container ships, are under construction, with the first in sea-trials. These measure at 400 m in length.

Anecdotally, from Appendix A we observe that 100 pixels is really not enough for a human observer to make much sense of the target vessel, in terms of shape and features. However, with enough pixels observable, the 3-m resolution image of the approximately 330 m long ship is still nevertheless seemingly adequate.

3.4 Unambiguous Range

Typical operation for many radars is to send out a pulse and receive the expected echoes before sending out the subsequent pulse. This places constraints on range vs. Doppler measurements for the ISAR system, otherwise significantly complicating the radar design and operation.

There is a fundamental trade in pulse-Doppler radar systems involving radar PRF. For a given PRF, there is a maximum unambiguous Doppler frequency, hence target closing velocity. For the same PRF there is a maximum unambiguous range. As PRF increases, unambiguous velocity increases, but unambiguous range decreases. Likewise, as PRF decreases, unambiguous velocity decreases, but unambiguous range increases.

We continue with the presumption that the effective pulse width of the ISAR is equal to the actual transmitted pulse width. For matched-filter pulse compression this is the case, and for 'stretch' processing (deramping followed by a frequency transform) this is nearly the case and more so for small range swaths compared with the pulse width.

By insisting that the echo return before the subsequent pulse is emitted, we insist that

$$\left(T_{eff} + \frac{2}{c}R\right) \le \frac{1}{f_p} \tag{38}$$

which can be manipulated to

$$R \le \frac{c(1-d)}{2f_p}. \tag{39}$$

The maximum R that satisfies this expression is often referred to as the 'unambiguous range' of the radar. Note the dependence on duty factor, d.

Note that there is no overt frequency dependence in this expression. However, we do recall from earlier analysis that the choice of PRF might in fact depend on the radar band in which we desire to operate. Nevertheless, once the PRF is chosen (along with the duty factor), the unambiguous range can be unambiguously calculated.

Figure 11 plots unambiguous range vs. PRF for several duty factors.

Recall that the PRF is chosen to keep target vessel feature velocities unambiguous. Clearly, we can sacrifice unambiguous velocity to enhance range. This is done by selecting the appropriate radar PRF.

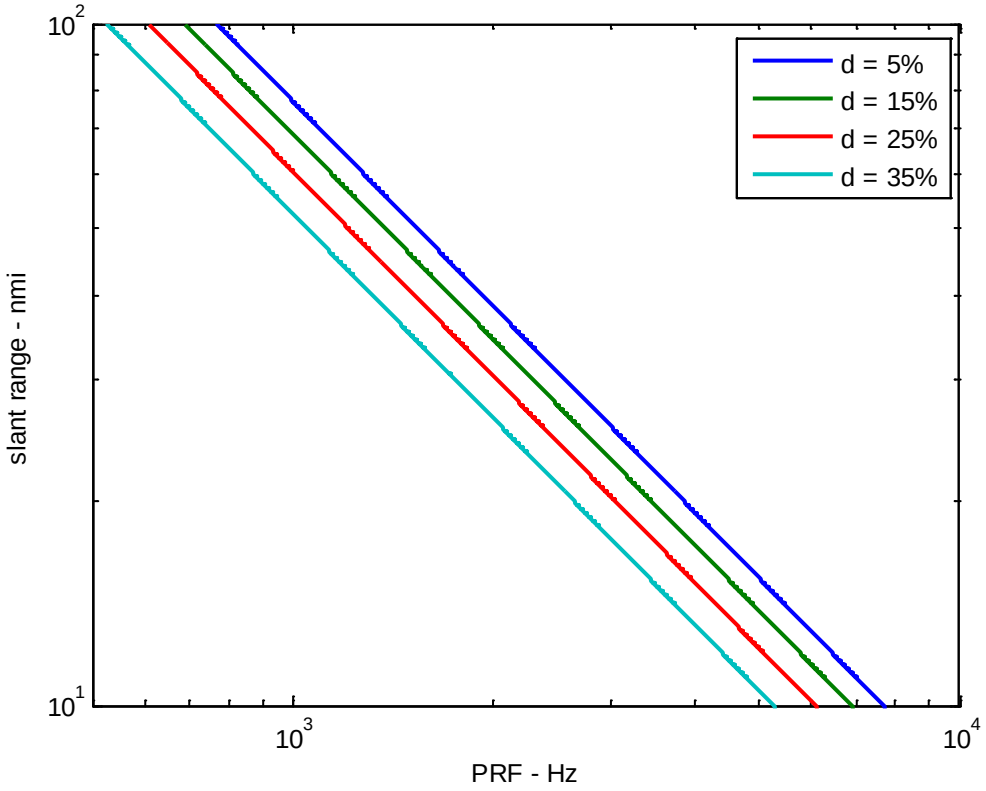

Figure 11. Unambiguous range limits vs. PRF.

If we need to work in the parameter space beyond the unambiguous range vs. PRF curves, then we need to either move along the curves (by appropriately modifying the radar PRF or duty factor), or we need to operate with pulses 'in the air', that is, transmitting new pulses before the expected arrival of a previous pulse's echo. This is entirely possible and is in fact routine in some radar systems, notably space-based systems. Resulting range ambiguities are resolved by appropriate phase coding or multiple-PRF schemes.

3.5 Range Migration

In an ISAR imaging, the modality is typically for the radar to dwell upon the target vessel for some extended period that encompasses perhaps many CPIs. Consequently, we define, or redefine, two time scales of interest to us, namely

$$T_{CPI} = \text{time interval of the CPI, and}$$
$$T_{dwell} = \text{time interval of the extended dwell.} \quad (40)$$

While a CPI may be limited to something on the order of 2-3 seconds, a dwell might be several or many tens of seconds. Our preference is for it to encompass at least one complete roll period of the target vessel.

The radar makes relative range measurements (relative to its own position), and also perhaps some degree of angular Direction of Arrival (DOA) measurements.

An airborne radar's own motion contributes range changes and perhaps target vessel perspective changes. The field of regard with respect to the aircraft's velocity vector of an ISAR mode may be in any direction, including broadside and directly fore or aft. This is unlike SAR, perhaps more like GMTI.

A maritime target vessel exhibits both translational motion, and angular motion with perhaps a large oscillatory rotational component. The translational motion provides the Doppler bias, or macro-Doppler, that yields vessel course and speed. The angular motion contributes to the micro-Doppler that allows us to resolve vessel features.

If the target vessel were to remain absolutely stationary, and the radar motion itself offered perspective changes during a CPI, then ISAR would devolve to simple SAR. Consequently, SAR can be entertained as perhaps a subset of the ISAR problem.

However, target vessels cannot be expected to be stationary, which means they eventually leave the neighborhood of their initial position at the start of an ISAR dwell. The ISAR system nevertheless desires for the entire target vessel to remain "in view" for the entire duration of the dwell. This means adjusting the "where" we look with the "when" we look there. This might require any or all of the following

1. Good knowledge of, and compensation for, the airborne radar motion,

2. Good knowledge of, and compensation for, the target vessel translational motion, and/or

3. Sufficient image size, including range swath extent.

We address these in turn.

3.5.1 Radar Motion

Knowledge of the radar's own motion will generally come from the radar's own navigator, for example perhaps a GPS-aided Inertial Navigation System (INS). Consequently, radar motion can be known with fairly good relative accuracy and precision.

The radar's own line-of-sight velocity towards the target vessel can be calculated as

$$v_{los,radar} = v_a \cos\psi_d \cos\theta_s , \tag{41}$$

where

v_a = forward velocity of the radar (assumed flying straight and level),
ψ_d = depression angle towards target vessel, and
θ_s = squint angle towards target vessel. (42)

These parameters can be assumed to be relatively constant during a CPI, but might change significantly over the course of a dwell. The worst case for ISAR is when angles are small, that is, looking forward or aft at shallow depression angles.

The range change due to radar motion during a dwell may be calculated as

$$\Delta R_{radar} = \bar{v}_{los,radar} T_{dwell} , \tag{43}$$

where

$\bar{v}_{los,radar}$ = some 'average' line-of-sight velocity due to the radar motion. (44)

For example, with a 30 second dwell with a 100 m/s line-of-sight velocity, the radar range will change by 3 km during the dwell due to radar motion alone.

3.5.2 Target Motion

The target vessel's bulk translational motion will generally not be known to the radar except from radar measurements themselves. For example, a tracker can estimate ship course and speed with some degree of accuracy and precision. The fidelity of target translational motion measurements will depend on the goodness of the track, which in turn depends on sensor data quality, track time, etc.

The target vessel's line-of-sight velocity away from the radar can be calculated as

$$v_{los,target} = -v_t \cos\psi_g \cos\theta_b , \tag{45}$$

where

v_t = forward velocity of the target vessel,
ψ_d = elevation angle towards radar, and
θ_b = relative bearing from ship to radar. (46)

The target vessel will also have a cross-range velocity calculated as

$$v_{cross,target} = -v_t \cos\psi_g \sin\theta_b, \tag{47}$$

As with aircraft motion, these parameters can be assumed to be relatively constant during a CPI, but might change significantly over the course of a dwell. The worst case for ISAR is when angles are small, that is, relative bearing from ship to radar being forward or aft at shallow elevation angles.

The range change due to target motion during a dwell may be calculated as

$$\Delta R_{target} = \bar{v}_{los,target} T_{dwell}, \tag{48}$$

where

$\bar{v}_{los,target}$ = some 'average' line-of-sight velocity due to the target motion. (49)

Some representative maritime vessel surface velocities are as follows.

$v_t \approx$ 10-17 kts average for typical bulk cargo ship,
$v_t \approx$ 21-25 kts voyage speed for large container ships,
$v_t \approx$ 25-27 kts maximum for typical cruise ship,
$v_t \approx$ 30+ kts maximum for destroyer,
$v_t \approx$ 33+ kts design for aircraft carrier,
$v_t \approx$ 40+ kts maximum for LCAC with full load,
$v_t \approx$ 48 kts maximum for Pegasus-class hydrofoil fast-attack patrol boats,
$v_t \approx$ 60 kts maximum for fastest high-speed ferry. (50)

Recall that to 4 significant digits, we may equate

1 kt = 0.5144 m/s. (51)

For example, with a 30 second dwell with a 30 kt line-of-sight velocity, the radar range will change by 463 m during the dwell due to target motion alone. This is substantially less than due to worst-case radar motion, but on the other hand the target's actual velocity is not known anywhere near as well as the radar motion.

3.5.3 Target Scene Size

For ISAR to image a target, the target must first be observable. That is, it must be illuminated by the antenna beam, and must reside within the range swath of the radar data as limited by timing and control. Furthermore, we desire the 'entire' target to remain in view during an entire dwell, not just a piece of it.

We shall presume that the range-extent of the field of view is limited principally by the range swath, rather than by the elevation pattern of the antenna beam. Furthermore, we must account for the grazing angle in converting ground-range to slant-range. Consequently, the scene diameter in ground-range is calculated as

$$D_y = \frac{D_r}{\cos\psi_g}, \tag{52}$$

where

$$D_r \text{ = slant-range swath.} \tag{53}$$

A more comprehensive calculation of the slant-range swath based on other radar parameters is beyond the scope of this report. However, we leave the reader with an anecdotal calculation that using stretch processing that employs a 2-k FFT, with 1 m resolution, we can probably count on a slant-range swath of perhaps 1.1 km.

The azimuth extent of the field of view is limited principally by the antenna beam footprint. We shall presume that no digital filtering will artificially reduce this. For a narrow antenna beam, we may calculate the azimuth scene diameter as

$$D_x = R\theta_{bw,az}, \tag{54}$$

where

$$\theta_{bw,az} \text{ = the azimuth beamwidth of the antenna (in radians).} \tag{55}$$

For example, at 10 nmi, a 3-degree antenna beamwidth will allow an azimuth scene diameter of 970 m. The same antenna will allow proportionately wider scenes at longer ranges.

We note that for the examples given, and with the largest ships exceeding 400 m in length, there is some margin. However we recall that the ship exhibits translational motion, for which our knowledge isn't perfect.

3.5.4 Target Tracker Accuracy

Our goal is to keep the target vessel within the field of view of the radar, both in range and in azimuth. To do this, we require an adequate understanding of the vessel translational motion, including position and velocity, in both range and azimuth. This is the job of a target tracker.

We shall presume that the radar motion is known perfectly, but the target vessel motion is not known perfectly, that is the tracker yields imperfect results. The question becomes "How accurate does the tracker need to be?"

The criterion for our answer is that we wish to limit the tracker error so that the entire target vessel remains in the field of view during the entire dwell, that is, the target vessel does not migrate out of the field of view. Towards this end, we desire

$$\begin{aligned} \bar{v}_{los,target,error} T_{dwell} &\le \frac{D_r}{2} - \frac{L_t}{2}\cos\psi_d \text{ , and} \\ \bar{v}_{cross,target,error} T_{dwell} &\le \frac{D_x}{2} - \frac{L_t}{2}, \end{aligned} \tag{56}$$

where

$$\begin{aligned} &\bar{v}_{los,target,error} \text{ = line-of-sight target velocity error,} \\ &\bar{v}_{cross,target,error} \text{ = cross-range target velocity error, and} \\ &L_t \text{ = length of the target vessel.} \end{aligned} \tag{57}$$

The velocity errors can be solved for explicitly as

$$\begin{aligned} \bar{v}_{los,target,error} &\le \frac{D_r - L_t\cos\psi_d}{2T_{dwell}} \text{ , and} \\ \bar{v}_{cross,target,error} &\le \frac{R\theta_{bw,az} - L_t}{2T_{dwell}}. \end{aligned} \tag{58}$$

For example, for the following parameters

$$\begin{aligned} &T_{dwell} \text{ = 30 s,} \\ &L_t \text{ = 300 m,} \\ &\psi_d \text{ = 10 deg.,} \\ &D_r \text{ = 1.1 km,} \\ &R \text{ = 10 nmi,} \\ &\theta_{bw,az} \text{ = 3 deg,} \end{aligned} \tag{59}$$

We may then calculate

$$\bar{v}_{los,target,error} \leq 13.4 \text{ m/s, and}$$
$$\bar{v}_{cross,target,error} \leq 11.1 \text{ m/s.} \quad (60)$$

Longer dwells require correspondingly more accurate velocity estimates. Longer ranges are more forgiving of cross-range velocity error. These error tolerances of course assume that an initial position estimate error is negligible, and the antenna footprint and range swath are adjusted continuously during the dwell to keep the target vessel centered in the field of regard.

We note that these errors are both greater than 20 kts, which is a fairly large percentage of the target vessel velocities listed earlier. In fact, for many vessels, for the parameters of our example we probably don't need much of a track at all. Of course the less is our error, probably the easier is the subsequent ISAR image formation processing.

Finally, we note that nothing prevents a tracker from updating and improving its track information during a dwell. However, we must ensure to avoid any phase discontinuities in the data during a dwell, especially if we employ overlapping CPIs.

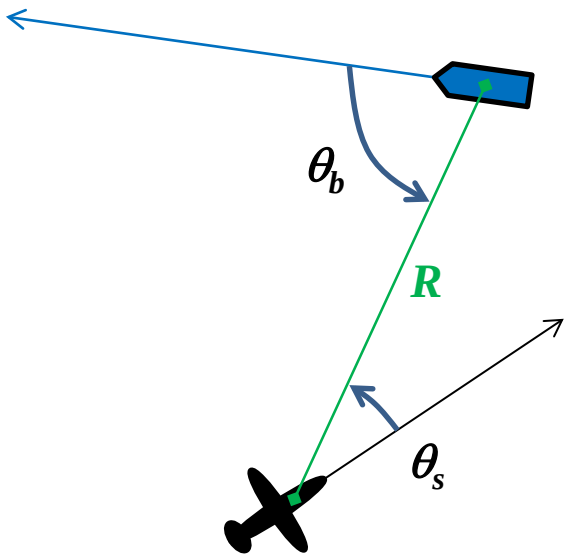

Figure 12. Plan view of radar and maritime target geometry.

3.6 Extending Range

Extending the range of an ISAR is equivalent to

1) ensuring that an adequate SNR is achievable at the new range of interest, and

2) ensuring that the unambiguous range constraint is adequately dealt with.

The unambiguous range issue was addressed in the last section. Here we address methods for increasing SNR at some range of interest.

We begin by writing the expression for SNR in the ISAR image as

$$SNR_{image} = \frac{P_{avg} G_A^2 \lambda^2 T_{CPI} \sigma}{(4\pi)^3 (kTF_N) L_{radar} L_r L_a} \left(R^{-4} 10^{\frac{-\alpha R}{10}} \right). \tag{61}$$

Note that SNR falls off as something greater than the 4th power of range.

This can be solved for noise equivalent RCS to yield

$$\sigma_N = \frac{(4\pi)^3 (kTF_N) L_{radar} L_r L_a}{P_{avg} G_A^2 \lambda^2 T_{CPI}} \left(R^4 10^{\frac{\alpha R}{10}} \right). \tag{62}$$

A discussion of increasing range for a particular noise equivalent RCS needs to examine how we can reduce the noise equivalent RCS to offset the effects of increasing range.

3.6.1 Increasing Average TX Power

We recall that the average TX power is the product of the peak TX power and the duty factor of the radar. Obviously we can increase the average power by increasing either one of these constituents, as long as it is not at the expense of the other. For example, a 100-W power amplifier operating at 30% duty factor is still better than a 200-W power amplifier operating at only a 10% duty factor, as far as SNR is concerned.

For a given TX power amplifier operating at full power, all we can do is ensure that we are operating at or near its duty factor limit. Since

$$P_{avg} = P_t d = P_t T_{eff} f_p \tag{63}$$

this is accomplished by increasing either or both the pulse width T_{eff} and the radar PRF f_p. If the radar PRF is constrained by an unambiguous range requirement, then the pulse width must be extended.

For ISAR employing stretch processing we identify

$$T_{eff} = \frac{I}{f_s} \tag{64}$$

where

I = the total number of (fast-time) samples collected from a single pulse, and
f_s = the ADC sampling frequency employed.

We note that to satisfy Nyquist criteria using quadrature sampling,

$$f_s \geq B_{IF} \tag{65}$$

where B_{IF} is the IF bandwidth of the radar.

Consequently, increasing the pulse width requires either collecting more samples *I*, or decreasing the ADC sampling frequency f_s (and the corresponding IF filter bandwidth B_{IF}).

Two important issues need to be kept in mind, however. The first is that extending the pulse width restricts the nearest range that the radar can image. That is, the TX pulse has to end before the near range echo arrives. The second is that the number of samples *I* restricts the range swath of the range-Doppler map to $(B_{IF} / f_s)I$ resolution cells. The consequence to this is that relatively wide swaths at near ranges requires lots of samples *I* at very fast ADC sampling rates with corresponding wide IF filter bandwidths.

At far ranges, where near-range timing is not an issue, for a fixed IF filter bandwidth and ADC sampling frequency, we can always increase pulse width by collecting more samples *I*. If operating near the unambiguous range, however, prudence dictates that we remain aware that increasing the duty factor does in fact reduce the unambiguous range somewhat.

Operating beyond the unambiguous range limit requires a careful analysis of the radar timing in order to maximize the duty factor, juggling a number of additional constraints.

Stretch processing derives no benefit from a duty factor greater than about 50%. A reasonable limit on usable duty factor due to other timing issues is often in the neighborhood of about 35%.

In any case, the easiest retrofit to existing radars for increasing average TX power (and hence range) are first to increase the PRF to the maximum allowed by the timing, and second to increase the pulse width, with a corresponding increase in number of samples collected.

Furthermore, we note that at times it may be advantageous to shorten the pulse and increase the PRF, even if it means operating with pulses in the air (beyond the reduced unambiguous range), just to increase the duty factor. This is particularly true when the hardware is limited the width of a pulse that can be transmitted.

In any case, doubling P_{avg} would allow increasing range by less than 19% even in clear weather.

3.6.2 Increasing Antenna Area

A bigger antenna (in either dimension) and/or better efficiency will yield improved SNR.

A larger elevation dimension will, however, reduce the illuminated swath width.

A larger azimuth dimension will also have the positive effect of narrowing the azimuth antenna beam width, thereby facilitating more accurate and precise target bearing determination, that is, target location. We note that although good for ISAR and GMTI, in a SAR system this will limit stripmap resolutions to coarser azimuth resolutions.

Of course, a narrower antenna beam also may require more diligence in keeping a moving vessel within the beam during a dwell.

In any case, doubling the antenna area would allow increasing range by 41% in clear weather, and something less in adverse weather.

3.6.3 Selecting Optimal Frequency

As previously discussed, there is a clear preference for operating frequency depending on range, altitude, and weather conditions. For example, at a 50-nmi range from a 25-kft AGL altitude with 4 mm/Hr rain, X-band offers a 2.4 dB advantage over Ku-band. For perspective, a 1-kW Ku-band amplifier would provide performance equivalent to a 575-W X-band amplifier (for the same real antenna aperture, efficiency, CPI time, etc...).

Choice of operating frequency does need to be tempered, however, by the factors noted earlier in this report.

Interestingly, there may even be significant differences within the same radar band. For example, at 25 kft AGL altitude, we can compare the top and bottom edges of the international Ku-band (15.7 GHz to 17.7 GHz). This is illustrated in Figure 13. At 10 nmi, the top edge achieves a 0.4 dB advantage. Parity is achieved at 13.7 nmi. Thereafter the bottom edge yields better SNR. The bottom edge advantage is about 2 dB at 30 nmi,

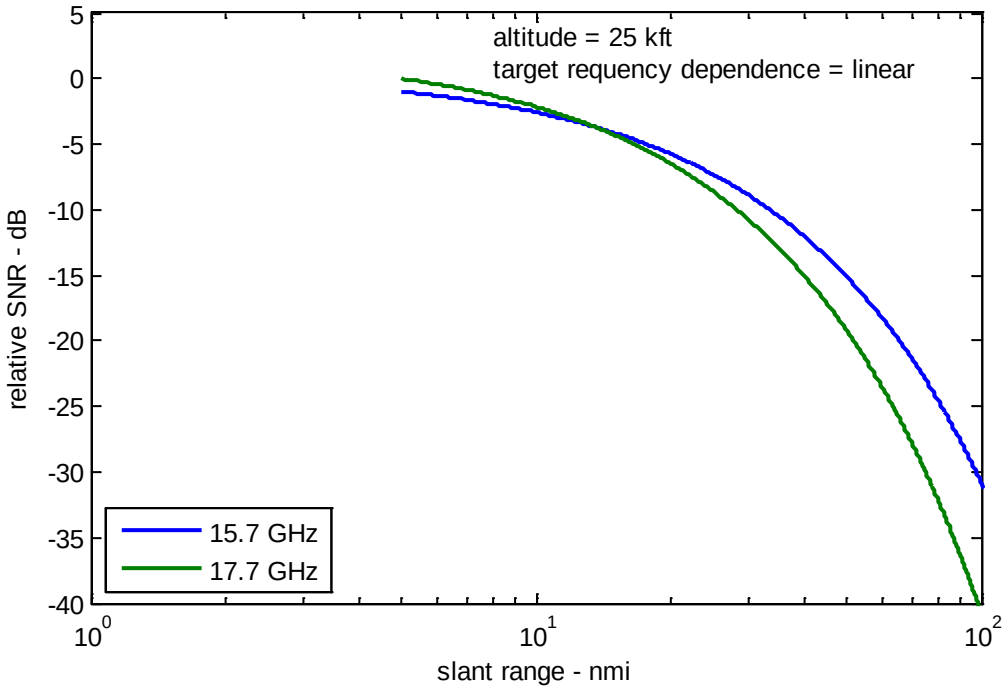

Figure 13. Relative performance at edges of Ku-band.

4 dB at 50 nmi, and nearly 10 dB at 100 nmi. Clearly, particularly at longer ranges, it seems advantageous to operate as near to the optimum frequency as the hardware and frequency authorization allow.

3.6.4 Modifying Operating Geometry

Once above the water-cloud layer, increasing the radar altitude will generally yield reduced average atmospheric attenuation, and hence improved transmission properties for a given range. Consequently, SNR is improved with operation at higher altitudes for any particular typical weather condition.

This translates to increased range at higher altitudes.

3.6.5 Longer CPI Time

Noise equivalent RCS is inversely proportional to the CPI time, T_{CPI}. Larger CPI times allow for larger SNR, and hence longer range.

Figure 14 illustrate a Ku-band example of how range-performance in both clear air and adverse weather depends on CPI times. Acceptable SNR performance is achievable to the left of the contours corresponding to a particular CPI time. Figure 15 corresponds to X-band with noise equivalent RCS adjusted for the difference in frequencies, assuming a linear relationship.

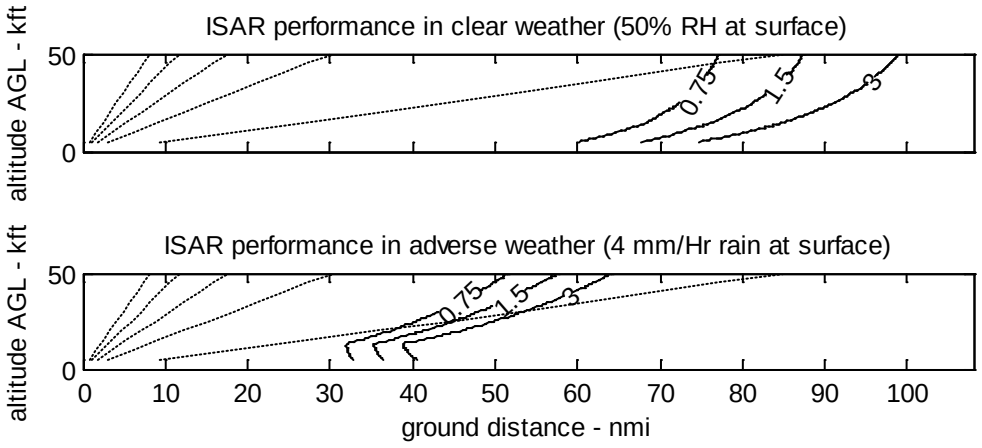

Frequency = 16.7 GHz	Noise RCS = 0 dBsm
Power (peak) = 400 W	Losses (signal processing) = 3 dB
duty factor = 0.35	Losses (radar) = 2 dB
Antenna (ap area) = 0.064826 sq m	Noise figure = 4 dB
Antenna (ap aspect) = 2	
Antenna (gain) = 31.0172 dB	(CPI time in "s")

Figure 14. Geometry limits vs. resolution for Ku-band. Contours are CPI times in seconds.

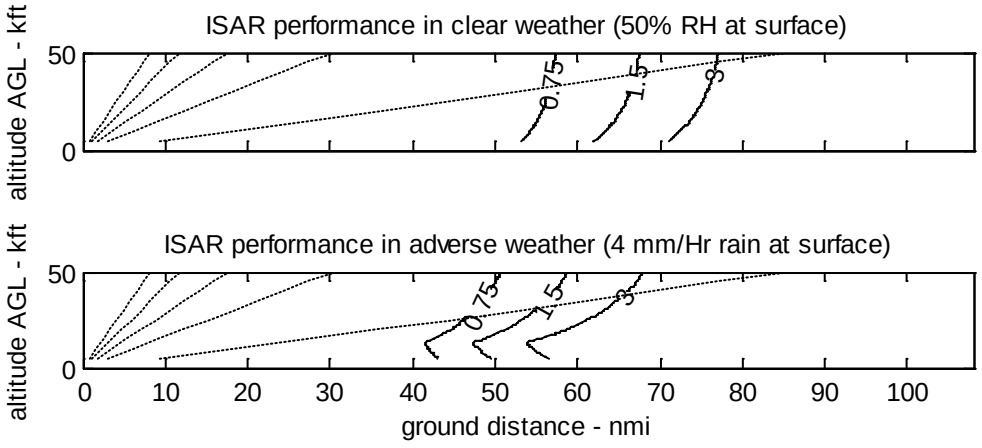

Frequency = 9.6 GHz	Noise RCS = -2.4045 dBsm
Power (peak) = 400 W	Losses (signal processing) = 3 dB
duty factor = 0.35	Losses (radar) = 2 dB
Antenna (ap area) = 0.064826 sq m	Noise figure = 4 dB
Antenna (ap aspect) = 2	
Antenna (gain) = 26.2083 dB	(CPI time in "s")

Figure 15. Geometry limits vs. resolution for X-band. Contours are CPI times in seconds.

3.6.6 Decreasing Radar Losses, Signal Processing Losses, and System Noise Factor

Any reduction in system losses yields a SNR gain of equal amount. This is also true of reducing the system noise factor. For example, reducing the TX amplifier to antenna loss by 1 dB translates to a 1-dB improvement in SNR. Likewise, a 2-dB reduction in system noise figure translates to a 2-dB improvement in SNR.

We note that high-power devices such as duplexers, switches, and protection devices tend to be lossier than lower power devices. Consequently, doubling the TX power amplifier output power might require lossier components elsewhere in the radar, rendering less than a doubling of SNR in the image. Furthermore, high-power microwave switches tend to be bulkier than their low-power counterparts, requiring perhaps longer switching times which may impact achievable duty factors.

As previously stated, the range processing loss due to window functions for sidelobe control can be eliminated by using appropriate waveforms, such as NLFM chirps.

3.6.7 Easing Weather Requirements

Atmospheric losses are less in fair weather than in inclement weather. Consequently SNR is improved (and range increased) for a nicer atmosphere. In real life you get what you get in weather, although a data collection might make use of weather inhomogeneities (like choosing a flight path or time to avoid the worst conditions).

Weather attenuation models are very squishy (of limited accuracy) and prone to widely varying interpretations. Consequently, ISAR performance claims might use this to advantage (and probably often do). The point of this is that while requests for proposals often contain a weather specification/requirement (e.g. 4 mm/Hr rain over a 10 nmi swath), there is no uniform interpretation on what this means insofar as attenuation to radar signals.

3.6.8 Changing Reference Noise Equivalent RCS

This is equivalent to the age-old technique of “If we can’t meet the spec, then change the spec.”

We note that a radar that meets a requirement for $\sigma_N = 0$ dBsm at some range, will meet a $\sigma_N = +10$ dBsm at some farther range. This is illustrated in Figure 16. SNR performance tends to degrade gracefully with range, consequently a tolerance for poorer ISAR performance will result in longer range operation. Poorer ISAR performance in this regard means a noisier ISAR image. Depending on what we might be looking for, data exhibiting a significantly higher noise equivalent RCS can still be quite usable.

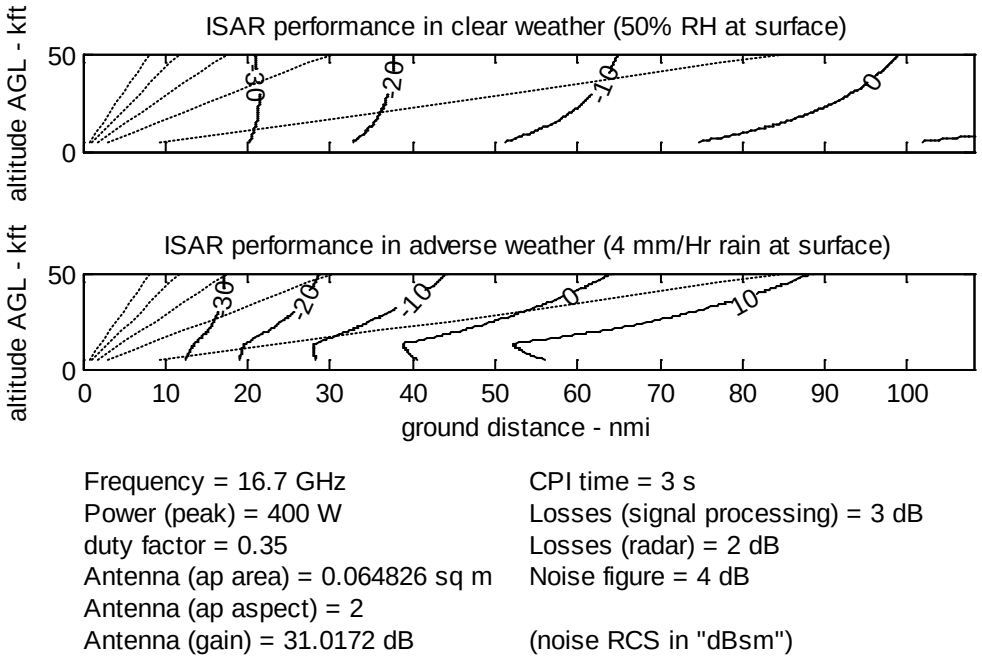

Figure 16. Geometry limits vs. noise equivalent RCS at Ku-band. Contours are noise equivalent RCS in dBsm.

Figure 17. Container ship Edith Maersk, launched in 2007, displacement 170794 gross tons, length 397 m, beam 56 m, maximum speed 26 kts. (image courtesy Wikimedia Commons/Heb)

3.7 Other Noise

The analysis in this report assumes that the only ‘noise’ that obfuscates the ISAR image is system ‘thermal’ noise. This is the target scene’s natural background emissions received by the antenna and supplemented by similar component noise in the radar itself, accounted for via the System Noise Figure.

Other ‘noise’ signals do exist in the radar, and can often be quite problematic, so much so that radar performance can be seriously degraded. These other noise sources often exhibit characteristics that are decidedly non-Gaussian, and non-white.

Such sources include, but are not limited to

Additive spurious signals (internal EMI)
External EMI
Multiplicative noise
Antenna sidelobe leakage
System RF channel nonlinearities
System I/Q imbalance
ADC Integral and Differential Nonlinearities
ADC Quantization Noise
Ambiguous range returns

Of course there are also a myriad of things in the processing that can screw things up, too.

Finally, we acknowledge that another source of ISAR image obfuscation is the sea clutter itself. This will be a function of sea-state and operating geometry. For low grazing angles and lower (more benign) sea-states, sea clutter echo energy will very often be below our noise threshold. At higher sea-states and steeper grazing angles, it may not always be so. In addition, sea clutter reflectivity is often frequency-dependent, manifesting brighter at higher radar operating frequencies.

“Change the way you look at things and the things you look at change.”
― Wayne W. Dyer

4 Conclusions

The aim of this report is to allow the reader to understand the nature of relevant physical parameters in how they influence ISAR performance. The radar equation can be (and was) transmogrified to a form that shows these parameters explicitly. Maximizing performance of a ISAR system is then an exercise in modifying the relevant parameters to some optimum combination. This was discussed in detail.

Nevertheless, some observations are worth repeating here.

A fundamental performance parameter is the concept of 'Noise Equivalent' RCS. This is the target RCS required for a 0 dB SNR. It is analogous to the Noise Equivalent Reflectivity for SAR.

Atmospheric losses are typically greater at higher frequency, in heavier rainfall, and at lower altitudes. These conspire to indicate an optimum operating frequency for a constrained antenna area at any particular operating geometry and weather condition.

Extending the range of an ISAR system can be done by incorporating any of the following:

increasing average TX power (peak TX power and/or duty factor)
increasing antenna area and/or efficiency
operating in a more optimal radar band (or portion of a radar band)
increasing CPI length (subject to coherence time limitations)
looking for brighter (higher RCS) targets
decreasing system losses and/or system noise figure
flying at a more optimal altitude (usually higher)
operate with a geometry such that the target has a higher RCS
operating in more benign weather conditions
allowing a higher noise floor

“The question is not what you look at, but what you see.”
— Henry David Thoreau

Appendix A – Noise Level in ISAR Image

Herein we present some anecdotal evidence regarding noise floor in an ISAR image. Figure 18 is a cropped segment of a Synthetic Aperture Radar (SAR) image of a large commercial freighter from a General Atomics AN/APY-8 Lynx Multi-Mode radar system, with the following parameters.

Ku-band
resolution = 3 m
pixel spacing ≈ 2.5 m
range ≈ 12.3 km
CPI time ≈ 0.8 s

The calm seas and relatively stationary vessel at a fairly near range allowed the SAR image of the approximately 330 m long ship to be fairly well focused, and representative of an ISAR image.

Figure 19 displays statistics of the original image. We note that the peak RCS value is 46 dBsm. Furthermore

163 pixels are at 20 dBsm or higher
360 pixels are at 15 dBsm or higher
631 pixels are at 10 dBsm or higher
993 pixels are at 5 dBsm or higher

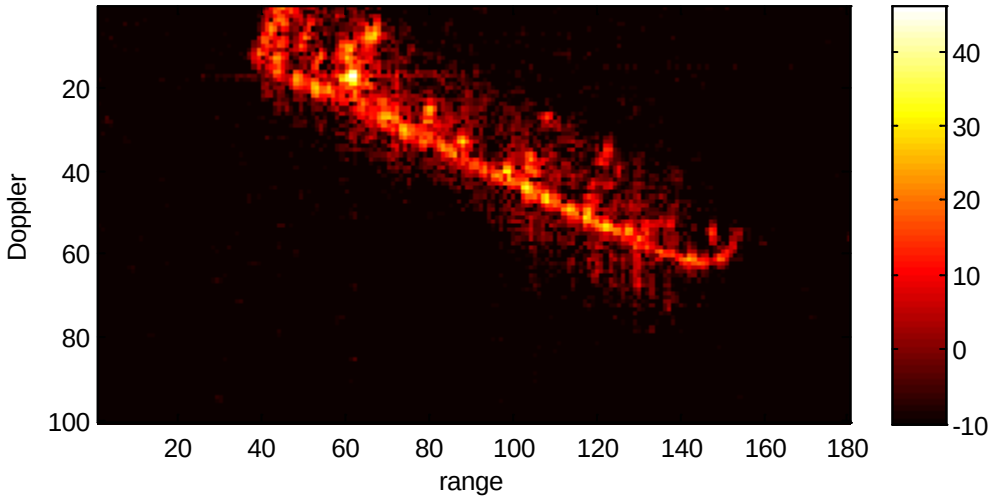

Figure 18. Original SAR image of ship near San Diego, CA. The colorbar denotes RCS in dBsm. Although the noise-equivalent RCS is about -39 dBsm, the ocean clutter level is at an average -18 dBsm value. (Courtesy of General Atomics Aeronautical Systems, Inc. All Rights Reserved.)

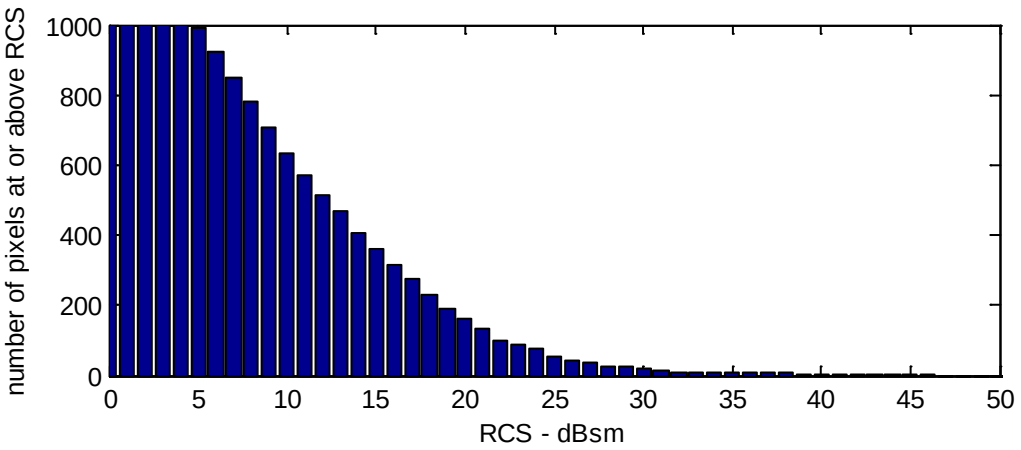

Figure 19. Pixel distribution statistics.

Images are rendered with various thresholds in Figure 20 through Figure 23. Although with a 20 dBsm threshold we already have more than 100 pixels on target, more features definitely become evident at lower thresholds, with most features evident with a 10 dBsm threshold. Assuming a 10 dB or better SNR for these features places the maximum allowable average noise level at 0 dBsm.

Figure 24, Figure 25, and Figure 26 artificially add increasing amounts of noise to the original image. As expected, most of the details in the original image are still visible in the 0 dBsm noise image. While the +10 dBsm noise image might still be useful, much of the detail has been lost with respect to the less noisy images.

This suggests that a performance-based range limit be consistent with a 0 dBsm noise level, at least for this target and others like it. We state without proof that SAR images of large ships docked in San Diego harbor, even at finer resolutions, suggest similar conclusions.

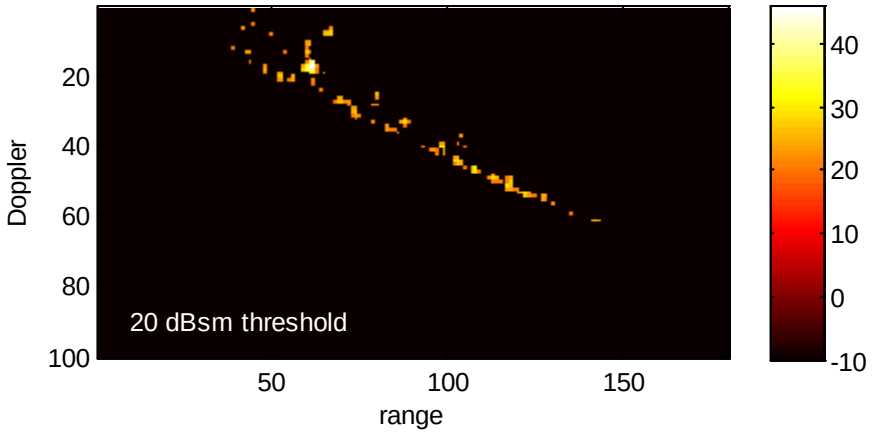

Figure 20. SAR image with pixel threshold of 20 dBsm.

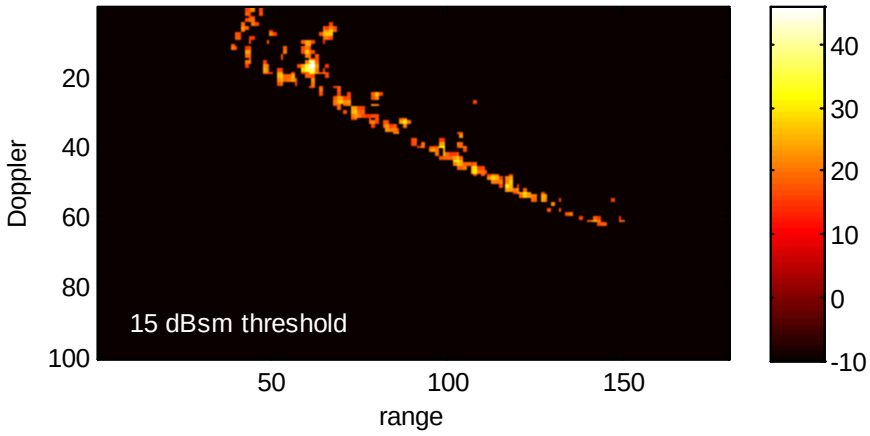

Figure 21. SAR image with pixel threshold of 15 dBsm.

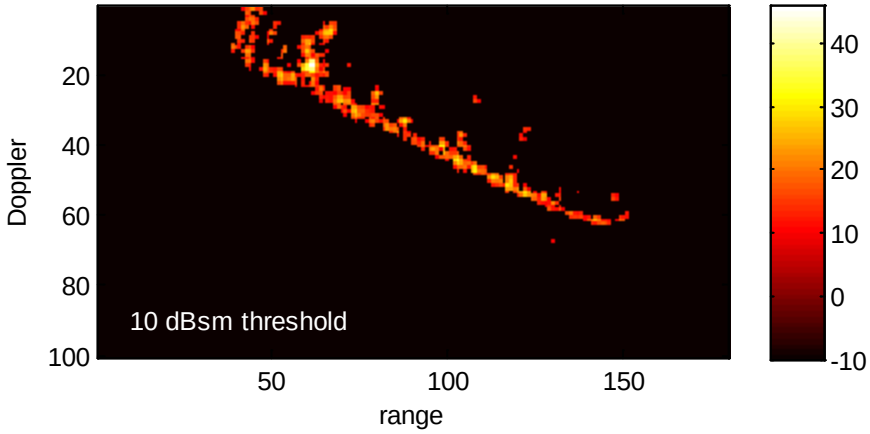

Figure 22. SAR image with pixel threshold of 10 dBsm.

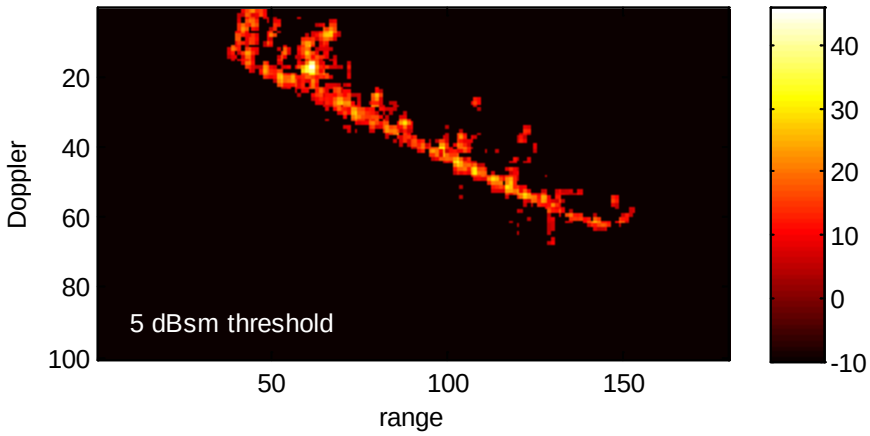

Figure 23. SAR image with pixel threshold of 5 dBsm.

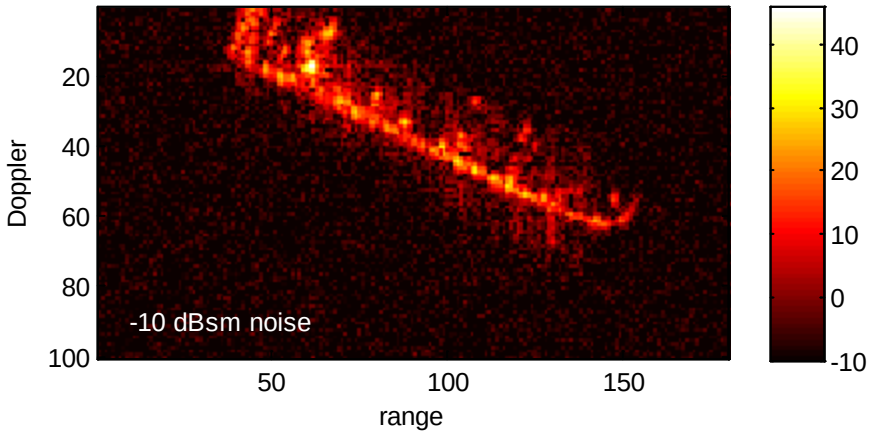

Figure 24. SAR image of Figure 18 with -10 dBsm added noise.

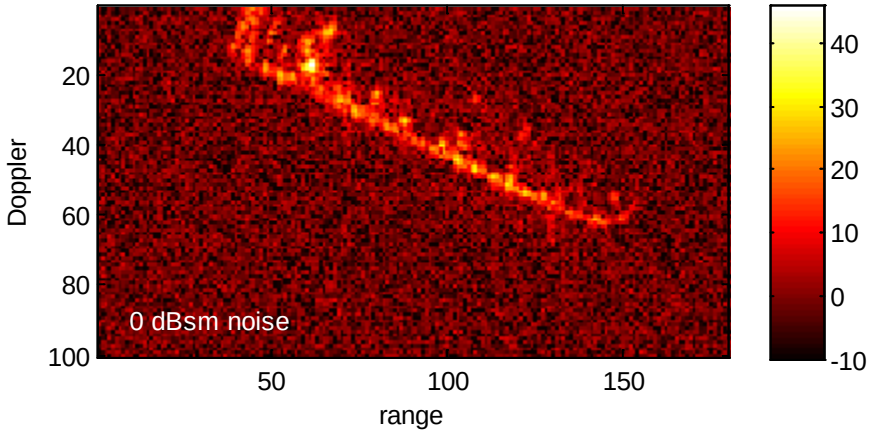

Figure 25. SAR image of Figure 18 with 0 dBsm added noise.

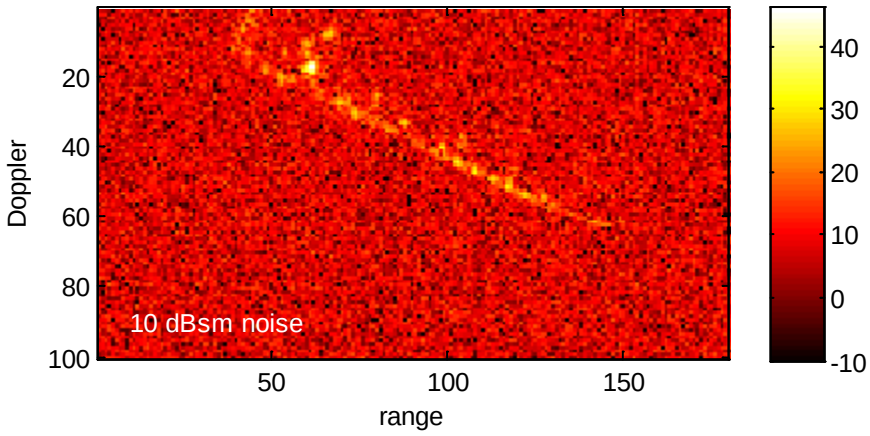

Figure 26. SAR image of Figure 18 with +10 dBsm added noise.

References

[1] Armin W. Doerry, "Performance Limits for Synthetic Aperture Radar – second edition", Sandia Report SAND2006-0821, Unlimited Release, February 2006.

[2] Armin W. Doerry, "Performance Limits for Exo-Clutter Ground Moving Target Indicator (GMTI) Radar", Sandia Report SAND2010-5844, Unlimited Release, September 2010.

[3] Armin W. Doerry, "Ship Dynamics for Maritime ISAR Imaging", Sandia Report SAND2008-1020, Unlimited Release, February 2008.

[4] A. W. Doerry, "What maritime ISAR designers should know about ship dynamics", SPIE 2012 Defense, Security & Sensing Symposium, Radar Sensor Technology XVI, Vol. 8361, Baltimore MD, 23-27 April 2012.

[5] Armin W. Doerry, "Radar Range Measurements in the Atmosphere", Sandia Report SAND2013-1096, Unlimited Release, February 2013.

[6] Armin W. Doerry, "Generating Nonlinear FM Chirp Waveforms for Radar", Sandia Report SAND2006-5856, Unlimited Release, September 2006.

[7] A. W. Doerry, "SAR Processing with Non-Linear FM Chirp Waveforms", Sandia Report SAND2006-7729, Unlimited Release, December 2006.

[8] Armin W. Doerry, Brandeis Marquette, "Shaping the Spectrum of Random-Phase Radar Waveforms", Sandia Report SAND2012-6915, Unlimited Release, September 2012.

[9] A. W. Doerry, B. Marquette, "Random-phase radar waveforms with shaped spectrum", SPIE 2013 Defense, Security & Sensing Symposium, Radar Sensor Technology XVII, Vol. 8714, Baltimore MD, 29 April – 3 May 2013.

[10] A. W. Doerry, "Atmospheric loss considerations for synthetic aperture radar design and operation", Proceedings of the SPIE 2004 Defense & Security Symposium, Radar Sensor Technology IX, Vol. 5410A, pp. 17-27, Orlando FL, 12-16 April 2004.

[11] A. W. Doerry, "Atmospheric attenuation and SAR operating frequency selection", Workshop on Synthetic Aperture Radar Technology", Redstone Arsenal, AL, October 22 & 23, 2003.

Distribution

Unlimited Release

1	MS 0519	J. A. Ruffner	5349	
1	MS 0519	A. W. Doerry	5349	
1	MS 0519	L. Klein	5349	
1	MS 0532	J. J. Hudgens	5240	
1	MS 0899	Technical Library	9536	(electronic copy)


Sandia National Laboratories